Published online April 12, 2018

Special Section: Stable Isotope Approaches in Vadose Zone Research

Core Ideas

- Bulk soil water isotopes have an evaporation signal, but mobile water isotopes do not.
- These differences are time variant and linked to the volume and age of the mobile water.
- Two pore domains (fast and slow) improve simulations of soil water isotope dynamics.
- A new model accounts for isotopic exchange via water vapor between two pore domains.
- This exchange is relevant for proper simulation of the evaporation signal in bulk soil water.

M. Sprenger, D. Tetzlaff, and C. Soulsby, Northern Rivers Institute, School of Geosciences, Univ. of Aberdeen, Aberdeen AB24 3FX, UK; D. Tetzlaff, IGB Leibniz Institute of Freshwater Ecology and Inland Fisheries, Humboldt Univ., Berlin, Germany; J. Buttle, School of the Environment, Trent Univ., Peterborough, ON K9L 0G2, Canada; H. Laudon, Dep. of Forest Ecology and Management, Swedish Univ. of Agricultural Sciences, Umeå, Sweden; H. Leistert and M. Weiler, Hydrology, Faculty of Environment and Natural Resources, Univ. of Freiburg, Freiburg im Breisgau, Germany; C.P.J. Mitchell, Dep. of Physical and Environmental Sciences, Univ. of Toronto, Scarborough, ON M1C 1A4, Canada; J. Snelgrove, Environmental and Life Sciences Graduate Program, Trent Univ., Peterborough, ON K9L 0G2, Canada. *Corresponding author (Matthias.sprenger@abdn.ac.uk).

Received 10 Aug. 2017.
Accepted 25 Nov. 2017.
Supplemental material online.

Citation: Sprenger, M., D. Tetzlaff, J. Buttle, H. Laudon, H. Leistert, C.P.J. Mitchell, J. Snelgrove, M. Weiler, and C. Soulsby. 2018. Measuring and modeling stable isotopes of mobile and bulk soil water. Vadose Zone J. 17:170149. doi:10.2136/vzj2017.08.0149

Measuring and Modeling Stable Isotopes of Mobile and Bulk Soil Water

Matthias Sprenger,* Doerthe Tetzlaff, Jim Buttle, Hjalmar Laudon, Hannes Leistert, Carl P.J. Mitchell, Jenna Snelgrove, Markus Weiler, and Chris Soulsby

Recent findings from stable isotope studies have opened up new questions about differences in the isotopic composition (δ^2H and δ^{18}O) of mobile (MW) and bulk water (BW) in soils. We sampled the isotopic compositions of MW using suction lysimeters and BW with the direct-equilibration method. The study was conducted at two landscape units in each of three catchments: the Bruntland Burn (Scotland), Dorset (Canada), and Krycklan (Sweden). We further used the numerical one-dimensional flow model SWIS (Soil Water Isotope Simulator) to simulate the hydrometric and isotopic dynamics. The model included evaporation fractionation, allowed differentiation between a fast and a slow flow domain, and included isotopic exchange via water vapor. Our measurements showed that MW plots along the local meteoric water lines, whereas BW plots below, which is indicative of evaporation fractionation. We suggest that the relative volume of MW to BW is relevant for explaining these isotopic differences because MW volumes are usually relatively low during periods of high evaporation. Under this condition, differences between MW and plant water isotopes are not paradoxical but rather related to the water that cannot be sampled with suction lysimeters but is still available for plant water uptake. The simulations accounting for fast and slow flow supported the conceptualization of the two soil pore domains with isotopic exchange via vapor exchange because this model setup resulted in the best model performance. Overall, these findings are of high relevance for current understanding related to the source and isotopic composition of water taken up by plants.

Abbreviations: BW, bulk soil water; LMWL, local meteoric water line; MAE, mean absolute error; MW, mobile soil water; OPD, one-pore domain; PET, potential evapotranspiration; TPD, two-pore domain with isotopic exchange via vapor exchange; TPD_noex, two-pore domain without isotopic exchange via vapor exchange; TWW, two water world.

Stable isotopes of hydrogen and oxygen in soil water (^{2}H and ^{18}O) are useful for identifying flow processes in the unsaturated zone (Garvelmann et al., 2012; Mueller et al., 2014; Oshun et al., 2016), understanding root water uptake patterns (Dawson and Ehleringer, 1991; Hervé-Fernández et al., 2016; McCutcheon et al., 2016; Volkmann et al., 2016; Rothfuss and Javaux, 2017), and calibrating hydrological models (Birkel et al., 2014; Sprenger et al., 2015b; Knighton et al., 2017). However, the various methods of soil water isotope sampling for isotopic analysis provide different information about water fluxes because they are sampling waters of different mobility (see review by Sprenger et al., 2015a). In particular, the differentiation between sampling that is limited to the mobile phase of soil water relative to sampling that includes water of a slower flow domain—the bulk soil water—has gained increasing attention. This interest stems from studies that showed that mobile water is similar to the infiltrating water of meteoric origin (precipitation), while bulk soil water samples exhibited an evaporation signal (Brooks et al., 2009; Goldsmith et al., 2012).

Mobile soil water is usually sampled with suction lysimeters, whereas the bulk soil water is most often sampled via cryogenic vacuum extraction (West et al., 2006; Koeniger et al., 2011; Orlowski et al., 2013) or the direct equilibration method in the laboratory (Wassenaar et al., 2008) or in situ (Rothfuss et al., 2013; Volkmann and Weiler, 2014).

While the differentiation of water mobility relating to these sampling methods is relatively long established (Araguás-Araguás et al., 1995; Landon et al., 1999; Figueroa-Johnson et al., 2007), it is still unclear why such pronounced contrasts in isotopic composition occur and how much interaction takes place between waters in different pore spaces (Vargas et al., 2017; Newberry et al., 2017). In particular, the kinetic fractionation, an altered $\delta^{18}O/\delta^{2}H$ ratio compared with the precipitation, is indicative of soil evaporation (Dansgaard, 1964) and observed in bulk soil water of upper soil layers in most vadose zone isotope studies (Sprenger et al., 2016b) but is usually not evident in mobile soil water.

The differences between mobile and bulk soil water isotopic composition (^{2}H and ^{18}O) motivated McDonnell (2014) to formulate the "two water world" (TWW) hypothesis, where mobile water is related to groundwater recharge and sources sustaining streamflow (with an isotopic composition similar to the precipitation input) and water of a slower flow domain is associated with plant water uptake (also referred to as ecohydrological separation). Based on this definition, Berry et al. (2017) recently presented hypothetical cases where mobile and bulk soil water would be isotopically different depending on the soil's moisture content and field capacity. However, it has not yet been assessed how mobile and bulk soil water volumes vary with time and how their relative proportions in the soil can be related to their isotopic composition.

There is an increasing interest in better understanding soil water isotope dynamics because isotope data have provided invaluable information for benchmarking hydrological models in the framework of celerities and velocities (McDonnell and Beven, 2014) at the plot (Haverd and Cuntz, 2010; Stumpp et al., 2012; Mueller et al., 2014; Sprenger et al., 2016c), hillslope (Windhorst et al., 2014), and catchment scales (Birkel et al., 2014; Soulsby et al., 2015; Knighton et al., 2017) to global land surface models (Haese et al., 2013; Wong et al., 2017). However, how waters of different mobility, like preferential flow (Beven and Germann, 2013), alter the bulk soil water isotopic composition is little understood and seldom accounted for in isotope modeling (e.g., Stumpp et al., 2007). A large-scale analysis of isotope fluxes by Good et al. (2015) argued that a differentiation between mobile and tightly retained waters (and their connectivity) was necessary to explain global isotope compositions of stream water and evaporation on continental scales. The variability of the stable isotopic composition of water held in different pore spaces (at different pressure heads)—potentially dividing the subsurface pool into two water pools—has not yet been considered in soil physical models.

This study aimed therefore to answer the following research questions:

1. Do mobile and bulk soil water isotope compositions differ with time, and if so, in what way?
2. What role does the relative volume of mobile to bulk soil water play in the interpretation of soil water isotope data?
3. How does the consideration of two pore domains in the subsurface affect hydrological modeling of soil water isotope dynamics at the plot scale?

We used observations of stable water isotopes in mobile and bulk soil waters in combination with soil moisture data to interpret differences in the mobile and bulk soil water at six locations in three long-term experimental catchments in the northern latitudes. We then applied a soil physically based model (SWIS, Soil Water Isotope Simulator) to each location, with a conceptualization of the subsurface assuming a uniform flow (one-domain flow) and another approach wherein the subsurface was divided into two pore domains to see how water held in a two-pore domain and its interactions via vapor exchange can influence the soil water isotope composition.

Methods

Mobile and Bulk Soil Water

In accordance with Berry et al. (2017), we define mobile water (MW) as soil water sampled using suction lysimeters (h_{MW} = 600 hPa in Fig. 1). The applied pressure head represents the limit at which water can be extracted with the suction lysimeter. Water held at higher pressure heads is therefore not included in these samples. This contrasts with what we define as bulk soil water (BW), which is soil water that was sampled using the direct-equilibration method as proposed by Wassenaar et al. (2008) and described below. While it is unknown how well the pore waters interact during the equilibration process of 2 or 3 d during the direct-equilibration method, we assume that water at pressure heads of 10^{6} hPa (h_{BW} in Fig. 1) will take part in the equilibration process.

We applied this concept of mobile and bulk soil water to six locations in three long-term experimental catchments, described in more detail below. Given that we know the water retention curve of a studied soil (Fig. 1, description of soil data below), we can infer the pressure head for a given measured soil moisture content [$\theta(t)$] according to van Genuchten (1980). We can then derive how much of the soil pore water can be sampled by suction lysimeters (V_{MW}) and how much is sampled with the direct-equilibration method (V_{BW}) by

$$\frac{V(t)_{MW}}{V_{Soil}} = \theta(t) - \theta(h_{MW}) \quad [1]$$

and

$$\frac{V(t)_{BW}}{V_{Soil}} = \theta(t) - \theta(h_{BW}) \quad [2]$$

In Fig. 1, we visualize V_{MW} (in blue) and V_{BW} (in red) for saturated conditions [$\theta(t) = \theta_s$] at one of the six locations (NF).

The fraction of mobile water relative to BW (V_{MW}/V_{BW}) varies as a function of soil moisture:

$$\frac{V_{MW}}{V_{BW}}(t) = \begin{cases} \theta(t)\left[\dfrac{1-\theta(h_{MW})}{1-\theta(h_{BW})}\right] & \text{for } \theta(t) > \theta(h_{MW}) \\ 0 & \text{for } \theta(t) \le \theta(h_{MW}) \end{cases} \quad [3]$$

Study Sites

The study includes data sets from three long-term research catchments in the northern latitudes: Bruntland Burn in the Scottish Highlands (57°2′ N, 3°7′ W), Dorset in south-central Ontario, Canada (45°12′ N, 78°49′ W), and Krycklan in northern Sweden (64°14′ N, 19°46′ E) (see map in Supplemental Fig. S1). These catchments are part of the VeWa (vegetation–water interactions) project, and their general hydro-meteorological characteristics were described by Tetzlaff et al. (2015).

All sites are characterized by a boreal landscape with a cold temperate climate. Mean annual temperatures and precipitation are 6°C and 1000 mm yr^{-1} for Bruntland Burn (Soulsby et al., 2015), 5°C and 1000 mm yr^{-1} at Dorset (Eimers and Dillon, 2002), and 1.8°C and 614 mm yr^{-1} at Krycklan (Laudon et al., 2013). There are extended periods of continuous snow cover at Dorset and Krycklan, with snow comprising 30% and 35 to 50% of annual precipitation at Dorset (Eimers and Dillon, 2002) and Krycklan (Laudon and Ottosson Löfvenius, 2016), respectively. At Bruntland Burn, usually <5% of annual precipitation is snowfall (Soulsby et al., 2015). Detailed descriptions of each study site were provided by Tetzlaff et al. (2014) for Bruntland Burn, by Buttle and Eimers (2009) for Dorset, and by Laudon et al. (2013) for Krycklan.

For this study, we focused on two sites within each experimental research catchment, where soil water at the 10-cm depth was sampled. At Bruntland Burn, soil water samples were taken in a Scots pine (*Pinus sylvestris* L.) forest (site identifier [ID]: NF) and beneath heather (*Calluna* spp. and *Erica* spp.) vegetation (site ID: NH) (Sprenger et al., 2017b). Sampling locations at Dorset were in red oak (*Quercus rubra* L.) (site ID: Or) and white pine (*Pinus strobus* L.) (site ID: Pw) stands. At Krycklan, the studied soils were along a transect, with one location covered by Norway spruce [*Picea abies* (L.) H. Karst.] and blueberry (*Vaccinium myrtillus* L.) 4 m away from a stream (site ID: S04) and the other with Scots pine and blueberry vegetation 22 m away from the stream (site ID: S22) (Table 1). The soils at the research catchments are organic rich and of loamy to sandy texture, with generally low (≤5%) clay content. Soil types are Podzols for five locations with organic matter content between 4 and 20%, while the soil at the near-stream location in Krycklan (S04) is characterized as a Histosol with about 80% organic matter content (Table 2). Within the considered 50-cm soil depth, two horizons were delineated at each site, with more organic matter in the upper horizon than the lower one. The two investigated landscape units at Bruntland Burn have been the subject of earlier studies (Geris et al., 2015b; Sprenger et al., 2017b), and previous work on the transect in Krycklan was reported by Stähli et al. (2001) and Peralta-Tapia et al. (2015).

Available Data

For each study site, soil water was sampled with two different methods to characterize the MW and BW isotope composition.

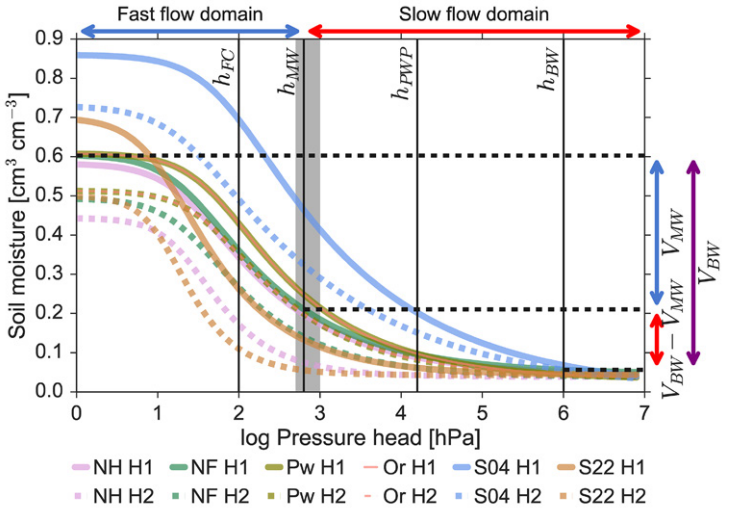

Fig. 1. Water retention curves for the six studied soils (H1 and H2 indicate the first and second soil horizons). The vertical lines indicate pressure heads at field capacity (h_{FC}), the limit of the suction lysimeter (here defining the mobile water, h_{MW}), the permanent wilting point (h_{PWP}), and the limit of water sampled with the direct equilibration method or cryogenic extraction, defined here as bulk soil water (water in fast flow domain + water in slow flow domain) (h_{BW}). The shaded area around h_{MW} indicates a range of pressure heads (500–1000 hPa) representing potential differences of suction lysimeters. The vertical arrows indicate the pore water volume that can be sampled with suction lysimeters (blue, V_{MW}) and with direct equilibration or cryogenic extraction (purple, V_{BW}) for fully saturated soil (pF 0; θ_s) for the water retention curve of the forested site at Bruntland Burn (NF). The water of the slow flow domain (red) is the difference between V_{MW} and V_{BW}. The horizontal arrows show the conceptualization of the fast and slow flow domains.

The sampling did not necessarily overlap, as listed in Table 2. The MW was sampled at each site at the 10-cm depth and in the second horizon (NF: 20 cm, NH: 30 cm, Pw: 40 cm, Or: 40 cm, S04: 45 cm, S22: 50 cm). At Bruntland Burn, MW was sampled every 2 wk in replicates of two using soil lysimeters (MacroRhizon by Rhizosphere Research Products). The pressure head was applied with a syringe in the morning, and water was sampled in the

Table 1. Vegetation characteristics of the six study sites.

Catchment	Site	Dominant vegetation cover	Rooting depth	Interception capacity	Canopy coverage
			cm	mm	%
Bruntland Burn	NF	Scots pine	50	7.5†	63‡
	NH	heather	15	2.65§	60‡
Dorset	Or	red oak	50¶	1.7	92#
	Pw	white pine	50¶	2.2	89#
Krycklan	S04	Norway spruce, blueberry	50††	1.3‡‡	95‡‡
	S22	Scots pine, blueberry	50††	1.3‡‡	95‡‡

† Haria and Price (2000).
‡ Can-Eye measurements (Soulsby et al., 2017).
§ Calder (1986).
¶ Field observations and Neary et al. (1987).
# Hemispheric photos with Can-Eye.
†† Blume-Werry et al. (2016).
‡‡ Stähli et al. (2001), from leaf area index (LAI) measurements derived from canopy coverage = 1 − exp(−0.463LAI).

Table 2. Characteristics of the studied soils. Soil texture is given according to USDA soil texture classes.

Catchment	Site	Soil type	Depth	Texture class	Sand	Silt	Clay	Organic matter	Bulk density	Mobile water sampling period	Bulk water sampling period
			cm		%				g cm^{-3}		
Bruntland Burn	NF	Podzol	0–15	loamy sand	78.9	17.1	4.0	80†	0.74†	23 Oct. 2012–27 Aug. 2013	29 Sept. 2015–23 Sept. 2016
			15–50	loamy sand	77.1	20.4	2.5	8†	1.04†		
	NH	Podzol	0–15	loamy sand	78.1	19.5	2.3	17	0.78†	1 June 2011–5 Nov. 2013	29 Sept. 2015–23 Sept. 2016
			15–50	loamy sand	81.9	16.2	2.5	3	1.25		
Dorset	Or/Pw	Orthic humo-ferric Podzol	0–25	sandy loam	67.9‡	28.6‡	3.5‡	3.9‡	0.65‡	23 June– 20 Oct. 2016	27 Oct. 2015–2 Nov. 2016
			25–50	sandy loam	67.6‡	31.6‡	1.2‡	2.7‡	0.87‡	30 June– 20 Oct. 2016	
Krycklan	S04	Histosol	0–35	organically dominated				40–70#		19 Jan.– 23 Nov. 2012	22 Sept. 2015–20 Sept. 2016
			35–50	sand	86§	14§	0§	10–40#			
	S22	Podzol	0–20	sand	91.3¶	8.2¶	0.5¶	<5#		15 Mar. 2012–20 Sept. 2016	22 Sept. 2015–20 Sept. 2016
			20–50	sand	95.2¶	4.4¶	0.4¶	<5#			

† Geris et al. (2015b).
‡ Soil description by Lozano et al. (1987).
§ Soil texture from the 70-cm soil depth from Nyberg et al. (2001).
¶ Nyberg et al. (2001).
# Lidman et al. (2017).

afternoon (Geris et al., 2015b). At Dorset, a pressure head (600 hPa) was applied to lysimeters in replicates of six, and the water was sampled 1 wk later. At Krycklan, the suction lysimeters were connected to a bottle under vacuum and sampled 2 to 3 d later at a monthly interval. While the sampling protocols and devices for the MW sampling were different at the three experimental catchments, their data are nevertheless comparable because they are all limited to sampling the mobile phase by applying a pressure head of about 600 hPa (h_{MW} in Fig. 1). All water samples were then analyzed by laser spectrometry (LGR DLT-100 laser liquid water analyzer for Bruntland Burn and Dorset, Picarro L1102-i and L2130-I for Krycklan) with accuracies better than ±1‰ for δ^2H and ±0.2‰ for $\delta^{18}O$. Samples flagged by the post-analysis software for organic contamination were filtered and reanalyzed.

The isotopic composition of the BW was determined using the direct-equilibration method proposed by Wassenaar et al. (2008). Soil samples were taken from 5- to 10- and 15- to 20-cm depths on 11 occasions at the Bruntland Burn, seven times at Dorset, and six times at Krycklan. A detailed description of the methodological procedure for the analysis of the samples from Bruntland Burn and Krycklan, performed at the laboratory of the Northern Rivers Institute, University of Aberdeen, was provided by Sprenger et al. (2017a). The analysis for the Dorset samples was performed at the Global Institute for Water Security, University of Saskatchewan according to the protocol of Hendry et al. (2015). Soil samples of 80 to 200 g were transported to the laboratory in sealed coffee bags (Weber Packaging) at the University of Aberdeen or in Ziploc bags at the University of Saskatchewan. In the laboratory, dry air was added to the bags, which were subsequently heat sealed and then stored under constant temperature for 2 d at the University of Aberdeen and 3 d at the University of Saskatchewan to allow the soil water to equilibrate with the headspace in the bags. After this equilibration period, the headspace vapor was directly sampled and analyzed by laser spectrometry (TWIA-45-EP LGR) and the δ^2H and $\delta^{18}O$ concentrations were determined. Equally treated bags filled with 10 mL of standard waters of known isotopic composition ranging across the expected isotopic composition in the soil samples enabled the vapor measurements of soil water isotopes to be related to the Vienna Standard Mean Ocean Water (in ‰). Because the analyses of BW isotopic composition were done with concordant methods, we believe the results are comparable even though they were conducted in different laboratories. The accuracy for this method was reported to be ±0.31‰ for $\delta^{18}O$ and ±1.13‰ for δ^2H (Sprenger et al., 2017b), and laser absorption changes due to CO_2 that developed in the bag during the equilibration did not occur (Sprenger et al., 2017a).

Daily precipitation, potential evapotranspiration (PET) derived via Penman–Monteith (Allen et al., 1998), mean air temperature (T), and relative humidity were available for all sites. Further, the isotopic composition (δ^2H and $\delta^{18}O$) of the precipitation on a daily basis was available at Bruntland Burn and Krycklan, and precipitation was sampled daily to every 2 wk at Dorset. Snowmelt isotopes were sampled with snow lysimeters at Krycklan and Dorset.

While snow usually plays a minor hydrologic role at Bruntland Burn (Ala-aho et al., 2017b), snowmelt dynamics for Dorset and Krycklan needed to be accounted for. For Dorset, observed snow dynamics, precipitation, and temperature data at the Beatrice climate station (http://climate.weather.gc.ca) (50 km east of the study sites) were used to calibrate a snowmelt model based on the day-degree method (Hock, 2003). Precipitation was assumed to be snow for $T < 0$°C, and snowmelt (SM) occurred on days with $T > 0$°C according to SM = DDF × T, where DDF is the day-degree factor. Calibration by optimizing the correlation between observed and simulated snow water equivalent resulted in DDF = 8.15 mm d^{-1} °C^{-1} and a significant correlation between observed

and predicted snow water equivalent ($r = 0.86, p < 0.05$). Inclusion of solar radiation did not improve the simulation of snowmelt dynamics. This snowmelt model was then applied to precipitation and temperature data from Dorset to estimate daily melt, while the isotopic composition of the meltwater was directly measured. At Krycklan, where the snowfall was regularly sampled and the isotopic composition determined, the melt dynamics and isotopic composition were simulated according to Ala-aho et al. (2017a). For the years when snowmelt was sampled with lysimeters (2012, 2015, and 2016), the measured isotopic composition was used instead of the simulated values.

We calculated the 30-d running mean of PET (PET_{30}) and the weighted running average isotopic composition of the precipitation and snowmelt input ($\delta^2H\ P_{30}$ and $\delta^{18}O\ P_{30}$) to relate these atmospheric variables to the observed soil water isotope data. For each experimental catchment, we computed the local meteoric water line (LMWL) as the regression line through the precipitation samples in a dual-isotope ($\delta^{18}O$ vs. δ^2H) plot. The LMWL is defined by the slope (a) and y axis intercept (b) as $\delta^2H = a\delta^{18}O + b$. With a known LMWL, we derived the line-conditioned excess (lc-excess) as proposed by Landwehr and Coplen (2006): lc-excess = $\delta^2H - a\delta^{18}O - b$. The lc-excess describes the deviation of a water sample from the LMWL in the dual-isotope plot, which is used to infer soil evaporation processes due to kinetic fractionation of precipitation input (McCutcheon et al., 2016; Sprenger et al., 2016b, 2017b).

Soil moisture content was monitored at each site at the 10-cm depth and in the second horizon (NF: 20 cm, NH: 30 cm, Pw: 40 cm, Or: 40 cm, S04: 45 cm, S22: 50 cm). At the Bruntland Burn sites, soil moisture was measured with time domain reflectometry (TDR) soil moisture probes (CS616, Campbell Scientific) at 15-min intervals from which daily averages were computed. Calibration of the sensors was done in the laboratory using bulk density and gravimetric water content measurements. At Dorset, instantaneous soil moisture measurements were performed using a Profile-Probe PR2 (Delta-T Devices) in parallel with the suction lysimeter sampling (six replicates at weekly intervals). For the two sites at Krycklan, daily average soil moisture values were derived from TDR measurements at 4-h intervals.

The soil physical characteristics, described by the water retention curve, were derived from pedotransfer functions by Schaap et al. (2001) for the Bruntland Burn and Dorset locations according to the soil textural and bulk density information listed in Table 2. For the Krycklan sites, the hydraulic conductivity, K, was based on soil core constant-head permeameter measurements by Nyberg et al. (2001) for soil samples from the 30- to 40-cm soil depth at S04 and 11 to 16 cm at S22. The Mualem–van Genuchten parameters α, n, and θ_r were defined by fitting with the RETC code (van Genuchten et al., 1991) to laboratory measurements by Nyberg et al. (2001). Maximum observed water content in long-term soil moisture time series served as θ_s for S04 and S22. All soil hydraulic parameters are listed in Table 3.

Canopy coverage at Bruntland Burn and Dorset was estimated using upward-facing hemispheric photographs input to the CAN-EYE software (Weiss and Baret, 2014), and leaf area index measurements were available at Krycklan (Table 1).

We applied the non-parametric Wilcoxon rank sum test to assess if MW and BW were significantly different at the 0.05 level between May and September, since the Shapiro-Wilk test for normality revealed that the data are not normally distributed.

Description of the Soil Water Isotope Simulator

In SWIS, water flow is simulated solving the Richards equation according to the Mualem–van Genuchten model (van Genuchten, 1980) and isotope transport is simulated according to the advection–dispersion equation. The model accounts for equilibrium fractionation according to Majoube (1971) and kinetic fractionation according to Gonfiantini (1986) during evaporation from the soil and interception storage as described by Mueller et al. (2014). The equations for the water flow and isotope transport are available in Mueller et al. (2014); we focus here on the description of the changes to the model since the application by Mueller et al. (2014).

In the current study, we used, in accordance with Barnes and Allison (1983), a dimensionless diffusion coefficient of 1 to account for diffusional transport in soil pores for the kinetic fractionation constants (28.4‰ for ^{18}O and 25.0‰ for ^2H; cf. Gonfiantini, 1986). For the isotope transport modeling, we converted isotope values in delta notation (δ^2H and $\delta^{18}O$ in ‰) to atomic ratios (C in %) for ^2H and ^{18}O. Note that in the following description, C always indicates that the calculation is done with atomic ratios for both ^2H and ^{18}O isotopes separately.

The Mualem–van Genuchten parameters for each soil horizon are listed in Table 3, and the dispersivity parameter required in the advection–dispersion equation was set to 10 cm for all sites based on the meta-analysis by Vanderborght and Vereecken (2007). The simulations were conducted for soil profiles reaching a depth of 50 cm, delineated into layers of 5-cm intervals.

Table 3. Soil hydraulic parameters describing the water retention curve (Fig. 1) and saturated hydraulic conductivity according to the Mualem–van Genuchten model: residual water content (θ_r), saturated water content(θ_s), air-entry value (α), shape parameter n, and hydraulic conductivity (K).

Catchment	Site	Horizon	θ_r	θ_s	α	n	K
			— $cm^3\ cm^{-3}$ —		cm^{-1}		$cm\ d^{-1}$
Bruntland Burn	NF	1	0.0454	0.6048	0.0434	1.3680	345.18
		2	0.0375	0.4936	0.0422	1.4542	322.89
	NH	1	0.0415	0.5822	0.0431	1.3765	392.46
		2	0.0387	0.4435	0.0452	1.7185	282.54
Dorset	Or/Pw	1	0.0456	0.6082	0.0221	1.3672	485.04
		2	0.0356	0.5136	0.0238	1.3937	427.09
Krycklan	S04	1	0	0.86	0.016	1.262	55.3†
		2	0.0002	0.73	0.0477	1.2381	80.4†
	S22	1	0.0429	0.70	0.0919	1.4895	147†
		2	0.0472	0.5	0.0835	1.7469	656†

† Lidman et al. (2017).

The upper boundary condition was defined by the input volume and isotopic compositions (δ^2H and $\delta^{18}O$) of precipitation or snowmelt and the output flux of evapotranspiration. The potential evapotranspiration was partitioned into potential transpiration and potential evaporation according to the canopy coverage (see Table 1) as suggested by Ritchie (1972). For NF, sap flow measurements were used to adjust the partitioning to the observations of Wang et al. (2017a), and at NH, evaporation estimates from a maximum entropy approach by Wang et al. (2017b) were used to adjust evaporation–transpiration partitioning. Soil evaporation was limited to the upper 10 cm because water losses are highest in this soil layer for coarse textures as described by Or et al. (2013). As proposed by Or et al. (2013), soil evaporation was subdivided into Stage 1, controlled by the liquid-phase continuity and capillary forces during wet conditions, and Stage 2, controlled by diffusion during dry conditions. Actual transpiration losses along the soil profile were limited to the rooting depths as listed in Table 1 and limited to depths and times when the pressure heads were below the permanent wilting point (h_{PWP}). While we have no data on the actual pressure head of the permanent wilting point, we used a commonly used value of pF 4.2 because the studied soils seldom reach such high pressure heads and transpiration demand is met by precipitation inputs most of the time (Wang et al., 2017a). Therefore, the uncertainty introduced by the assumed h_{PWP} = 15,000 hPa is expected to be low. Evaporation and transpiration each decreased linearly with depth.

Precipitation input was partitioned into direct infiltration and interception according to the canopy coverage (Table 1). When the interception capacity was reached (listed in Table 1), the surplus infiltrated into the soil. Evaporation from interception storage led to isotopic fractionation, and precipitation entering the interception storage mixed with water stored prior to the rainfall. In contrast to evaporation, transpiration was not associated with isotopic fractionation and thus did not enrich the soil water. Interception storage was set to zero during snowfall and snowmelt because snowmelt infiltration volumes were simulated and their isotopic compositions were available from either measurements or simulations as described above.

The SWIS model was applied in the current study assuming either an equilibrium model (one-pore domain, OPD) or non-equilibrium model (two-pore domain, TPD). The OPD assumed uniform flow, but the TPD divided the subsurface into two pore domains according to the definitions of MW and BW above and visualized in Fig. 1 and 2. Input and output of the TPD were divided with respect to their relative pore volumes. If the pore volume of the slow flow domain was filled, it was routed to the fast flow domain. The setup of the TPD approach was similar to the dual-permeability approach of Gerke and van Genuchten (1993), but in SWIS, the same set of Mualem–van Genuchten parameters is used in the two domains and there is no isotopic exchange between the fast and slow flow domains via the liquid phase. Instead, isotopic exchange between the fast and slow flow domains occurs via vapor exchange (Fig. 2). As described by

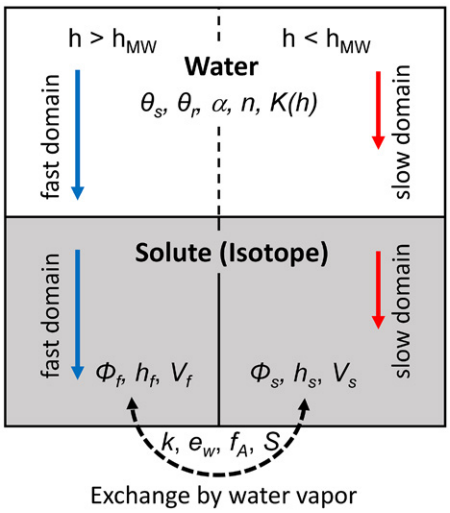

Fig. 2. Conceptualization of the two-pore domain approach of the model SWIS. The fast and slow pore domains are divided according to the pressure head (see Fig. 1), but the water flow of both domains is described by the same set of Mualem–van Genuchten parameters. The exchange between the fast and slow domain via water vapor is described in Eq. [4–7]; h is pressure head, h_{MW}, is pressure head limit of "mobile water," θ_r is residual water content, θ_s is saturated water content, α is air-entry value, n is a shape parameter, K is hydraulic conductivity, h_f and h_s are pressure heads in the fast and slow flow domains, respectively, V_f and V_s are soil water volumes in the fast and slow flow domains, respectively, ϕ_f and ϕ_s are soil porosities of the fast and slow domains, respectively, k is a parameter for exchange via water vapor, e_w is saturated vapor pressure, f_a is an areal factor that scales the surface area of the liquid–vapor interface, and S is a packing parameter for the surface area model.

Criss (1999), two water pools of different isotopic composition approach their weighted mean (C_{eq}) due to exchange via water vapor exchange at equilibrium.

In the SWIS model, this equilibrium concentration follows the mixing model between the volume of water in the fast and slow flow domains (V_f and V_s, respectively) (cm^3) and their isotopic composition (C_f and C_s, respectively) (%):

$$C_{eq} = \frac{V_f C_f + V_s C_s}{V_f + V_s} \quad [4]$$

How fast this equilibrium is reached depends, according to Criss (1999), on the vapor pressure (e_w) (hPa), the water volumes (V_f and V_s), and the surface area where the liquid–vapor exchange happens in the fast and slow flow domains (A_f and A_s, respectively) (cm^2):

$$C_j(t) = C_{eq} + \exp\left(-k\frac{A_f A_s}{A_f + A_s}\frac{V_f + V_s}{V_f V_s}e_w t\right)\left[C_j(t) - C_{eq}\right] \quad [5]$$

with C being atomic ratios of ^2H or ^{18}O isotopes, and the subscript j representing the fast or slow pore domain. The parameter k (cm hPa^{-1} d^{-1}) is set to 0.0060376 based on Ingraham and Criss (1998), e_w (hPa) is defined according to the Clausius–Clapeyron equation (Warneck and Williams, 2012), and t (d) is the time step.

The water volumes (V_f and V_s) result from the water flow calculations based on the Richards equation.

The surface area for the liquid–vapor exchange is conceptualized in SWIS by assuming that the pore domains are each a single tube. Based on the capillary rise equation [$r = -2\sigma/(\rho_w h)$], with σ the surface tension (=7.27 × 10^{-2} J m^{-2} at 20°C) and ρ_w the water density (=1 g cm^{-3}), we can derive from the pressure heads (h_s and h_f, respectively, in 1 hPa = 0.01 J g^{-1}) the radii (cm) of the two pore domains as $r_s = -0.14\ m^3\ s^{-2}/h_s$ and $r_f = -0.14\ m^3\ s^{-2}/h_f$ (Campbell, 1985). The water volume then defines the length of the tube, and the exchange surfaces, covering only part of the surface tube, are a function of porosity (ϕ_f and ϕ_s, dimensionless), the dimensionless packing (S), and the water content of the slow and fast domains (V_s and V_f) as

$$A_s = \frac{\phi_s^{f_A} S V_s 2}{r_s} \quad [6]$$

$$A_f = \frac{\phi_f^{f_A} S V_f 2}{r_f} \quad [7]$$

with f_A being a factor to adjust the area of exchange between liquid and vapor (dimensionless). For the parameter representing the packing, S, the value of 0.15 was chosen as a mean value because uniform spherical particles would yield between ~0.09 (for the densest packing) and ~0.21 (for the loosest packing).

We applied the model using the representation of uniform flow (OPD) and using the TPD, where the areal factor was set to $f_A = 4$ to allow forexchange between the pore spaces. We further tested the two-pore domain approach with $f_A = 10$, impeding any isotopic interaction between the mobile and tightly retained soil waters (TPD_noex). To assess the sensitivity of the TPD approach to the assumed pressure head defining the fast and slow flow domains (Fig. 1), we ran the TPD approach additionally with h_{MW} = 500 hPa and h_{MW} = 1000 hPa.

In addition to the SWIS simulations, we also ran simulations with a modified HYDRUS-1D that does not account for isotopic fractionation processes. However, we used a modified HYDRUS version, where the solute (in our case the isotopic composition) does not evapoconcentrate at the upper boundary (Stumpp et al., 2012). Further, HYDRUS-1D cannot split the soil water into fast and slow flow domains according to defined pressure heads, which we aimed to simulate in our study.

All simulations started for Krycklan on 1 Jan. 2010 and for Bruntland Burn and Dorset on 1 June 2011, and ended on 30 Sept. 2016. The goodness of fit for the model approaches were assessed for the different sites with the mean absolute error (MAE) and the Pearson correlation coefficient comparing the simulated soil moisture, δ^2H, and lc-excess of MW and BW and the average values of soil moisture and the MW and BW δ^2H and lc-excess, respectively. We decided to use the MAE and not the root mean square error because we cannot expect that the residuals between simulated and observed isotope and soil moisture data follow a normal distribution, which would be a requirement for the latter (Chai and Draxler, 2014). Because our sample size of observations was relatively low, we could not compare the simulations using the Nash–Sutcliffe efficiency (NSE, Nash and Sutcliffe, 1970) or Kling–Gupta efficiency (KGE, Gupta et al., 2009). Using the MAE as a goodness-of-fit measure limits the comparison of simulations to average values of observed data. However, mean values do not reflect the high heterogeneity present in the soil water isotopic composition. Therefore, we included the variability of hydrogen and oxygen stable isotopes of soil water, δ^2H and $\delta^{18}O$, in the assessment of our model performances for the BW data that were taken in replicates of five for each sampling day. To do so, we estimated the probability density function for both BW δ^2H and BW $\delta^{18}O$ leading to a bivariate approximation of the variability in the dual-isotope space.

Results

Observed Differences between Mobile and Bulk Soil Water Isotopes

Mobile (MW) and bulk soil water (BW) δ^2H and $\delta^{18}O$ compositions at the 10 cm depth at the six locations generally reflected the isotopic composition of precipitation and snowmelt at each site according to latitude. Soil water between May and September was most enriched in δ^2H at Bruntland Burn, less enriched at the Dorset locations, and considerably depleted at the Krycklan sites (Fig. 3a). The δ^2H and $\delta^{18}O$ values of MW were not significantly different from values of BW samples; however, S22 was an exception, where MW was significantly depleted in ^2H compared with BW. In contrast, we generally observed a significantly lower lc-excess for BW

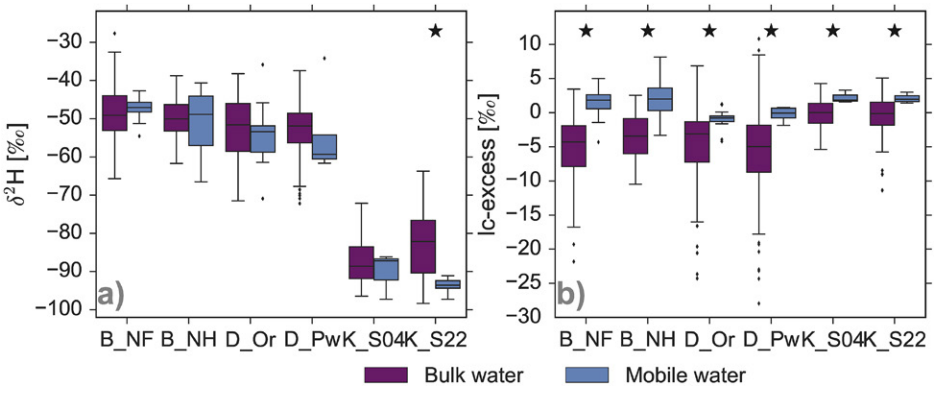

Fig. 3. Comparison between the (a) δ^2H and (b) the line-conditioned excess (lc-excess) of the bulk soil water and the mobile soil water at the 10-cm soil depth for the May to September period at the six sites. Significant differences between mobile water and bulk water for each site are indicated by stars (Wilcoxon rank sum test, $p < 0.05$).

than for MW at all locations for samples taken during the growing season (Fig. 3b). Thus, there was a soil evaporation signal in BW but not in MW, whose lc-excess was generally close to zero. While we do not expect intense evaporation during the dormant season, the sampling strategies were also too different to include this period to check for similarities in soil water lc-excess values.

Temporal dynamics of the soil water isotope compositions are shown in the dual-isotope plots in Fig. 4 (and in time series in Supplemental Fig. S2 and S3). The MW isotopic compositions for all six landscape units generally plotted along the LMWL (circles in Fig. 4). Suction lysimeter samples were therefore water that did not undergo evaporation after infiltration into the soil. For the BW, only samples taken during winter and spring plotted along the LMWLs (blue and green stars in Fig. 4). In contrast, BW samples from summer and autumn plotted partly below the LMWL, along an evaporation line (linear regression through samples) with slopes between 2.7 and 6.8 during summer (red stars in Fig. 4).

For most sampling locations, the δ^2H and $\delta^{18}O$ values of MW and BW at 10 cm followed the precipitation and snowmelt input isotopic composition averaged across 30 d prior to sampling (Table 4). While δ_{BW} was correlated at all locations with δ_{P30} ($r > 0.51$), δ_{MW} did not show a relationship with δ_{P30} at the Krycklan locations. Limiting the correlation of the soil water isotopic composition to the immediate antecedent infiltrating water (P_1 δ^2H in Table 4) resulted in significant relationships only for the MW at Dorset sites. For all other locations, the correlation coefficients were reduced compared with the relationship of MW δ^2H and BW δ^2H to the long-term average of P_{30} δ^2H. Thus, the soil water did not simply reflect short-term effects of recently infiltrated water, but rather both MW and BW mainly comprised a mixture of younger (most recent infiltration) and older water (infiltrated a few weeks to months previously). This is further supported by the dampened variability in the MW and BW isotopic compositions compared with the precipitation input

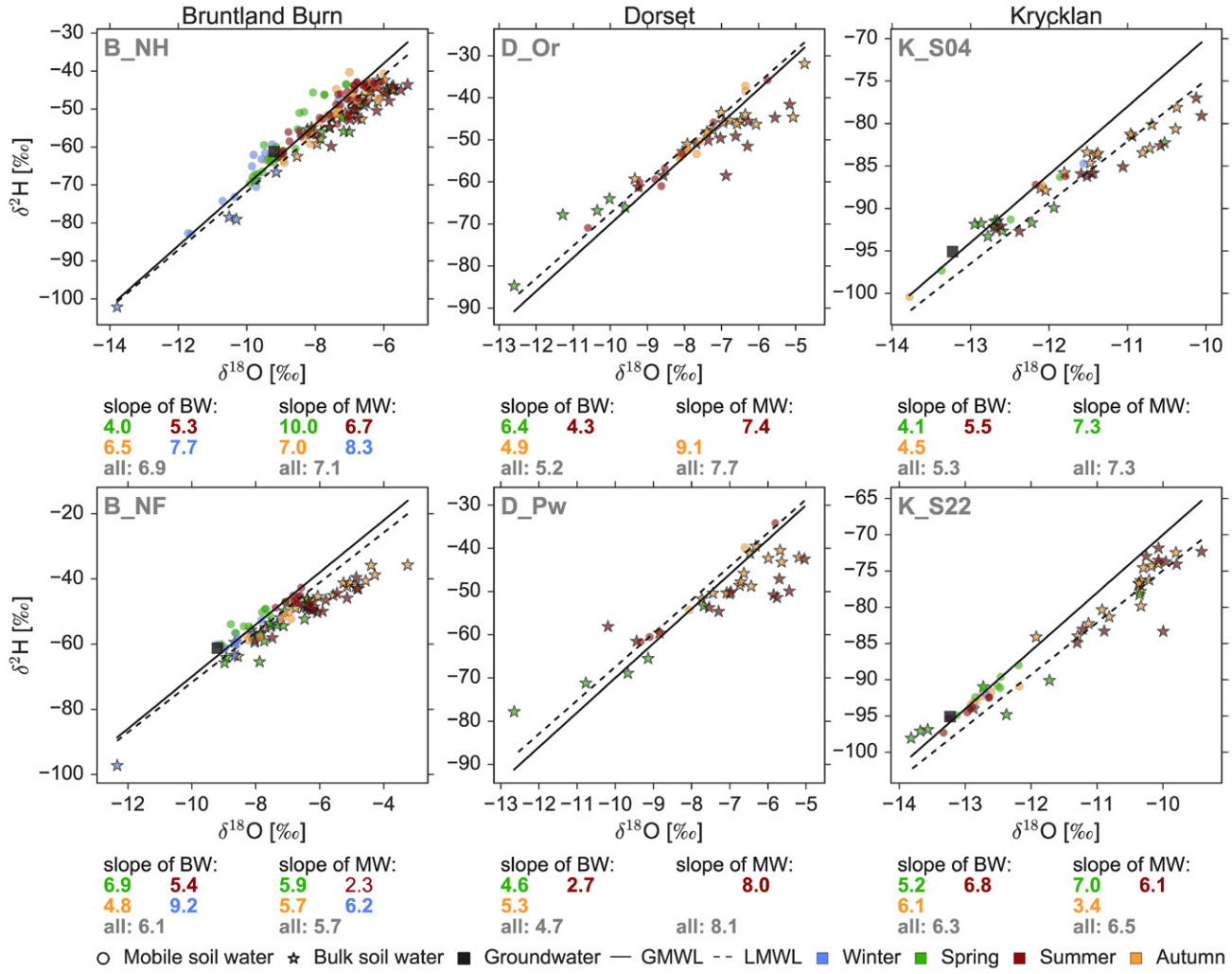

Fig. 4. Dual isotope plots comparing mobile (MW, circles) and bulk (BW, stars) soil water samples at the 10-cm soil depth. Color code indicates the season. Also shown are the global meteoric water line (GMWL, black line), the local meteoric water line (LMWL, dashed line), and the groundwater (black squares) for Bruntland Burn (data from Birkel et al., 2014) and Krycklan (data from Peralta-Tapia et al., 2015). The LMWL for Bruntland Burn: $\delta^2H = 7.7\delta^{18}O + 4.9$; for Dorset: $\delta^2H = 7.8\delta^{18}O + 10.1$; for Krycklan: $\delta^2H = 7.2\delta^{18}O - 3$. Slopes of the regression lines for the BW and MW samples are given for each season indicated by the font color and for all samples in gray.

Table 4. Pearson correlation coefficients between soil water isotopic composition at the 10-cm soil depth and line-conditioned excess (lc-excess) for mobile soil water (MW) and bulk soil water (BW) and atmospheric drivers prior to soil water sampling: input signal (precipitation and snowmelt) weighted averages over 30 and 1 d (P_{30} and P_1, respectively), average evapotranspiration over 30 d (ET_{30}), and soil moisture content (θ).

Site	MW δ^2H vs. P_{30} δ^2H	BW δ^2H vs. P_{30} δ^2H	MW δ^2H vs. P_1 δ^2H	BW δ^2H vs. P_1 δ^2H	MW lc-excess vs. ET_{30}	BW lc-excess vs. ET_{30}	MW lc-excess vs. θ	BW lc-excess vs. θ
NF	0.60**	0.87**	0.48	0.30	−0.16	−0.52	0.74**	0.49
NH	0.56**	0.65*	0.08	0.31	−0.25	−0.59*	0.31**	0.33
Or	0.63*	0.67	0.70*	0.48	−0.15	−0.56	0.03	0.99**
Pw	0.99**	0.69	0.89*	−0.03	−0.24	−0.37	0.53	0.90
S04	0.06	0.49	−0.13	−0.22	0.25	−0.15		
S22	−0.28	0.96**	−0.30	0.38	−0.60	−0.41		

* Significant at $p < 0.05$.
** Significant at $p < 0.01$.

composition (Supplemental Fig. S2). The lowest δ_{BW} and δ_{MW} temporal dynamics were found for the near-stream location at Krycklan (S04), where the δ_{MW} barely changed despite a variable input signal (Table 4).

The S04 location also showed the poorest relationship between BW lc-excess and average evapotranspiration 30 d prior to the sampling (PET_{30}). However, BW lc-excess at all sites decreased with increasing PET_{30} (Table 4). The BW lc-excess was generally lower than the P_{30} lc-excess, indicating the effect of some kinetic fractionation due to soil evaporation. In contrast to BW, the MW lc-excess did not vary with time or exhibit a relationship with PET_{30}. The BW lc-excess significantly decreased with decreasing soil moisture at the Dorset sites and to a lesser extent at the Bruntland Burn sites (Table 4). Missing data for the Krycklan soil moisture measurements precluded an analysis of this relationship, but no relationship with soil moisture is expected because BW lc-excess showed little variation at these sites.

For Dorset, where MW and BW were sampled during the same period, the differences between BW lc-excess and MW-lc-excess increased with decreasing soil moisture ($r = 0.94$, $p = 0.056$ for Or; $r = 0.86$, $p = 0.14$ for Pw). Also for the Krycklan site S22, MW and BW were sampled in parallel on 6 d, and the δ_{BW} was more enriched than δ_{MW} during summer but was about the same after snowmelt.

Temporally Variable Mobile and Bulk Soil Water Volumes

As shown in Fig. 1, sampling with suction lysimeters considers a smaller volume than the soil water volume accounted for in isotope analysis with direct equilibration or cryogenic extraction. Using the measured soil moisture at the six locations and the two different horizons of the considered profiles, we can use the water retention curves in Fig. 1 to derive time series of pressure heads at these sites (Fig. 5a). Pressure head showed a strong seasonality

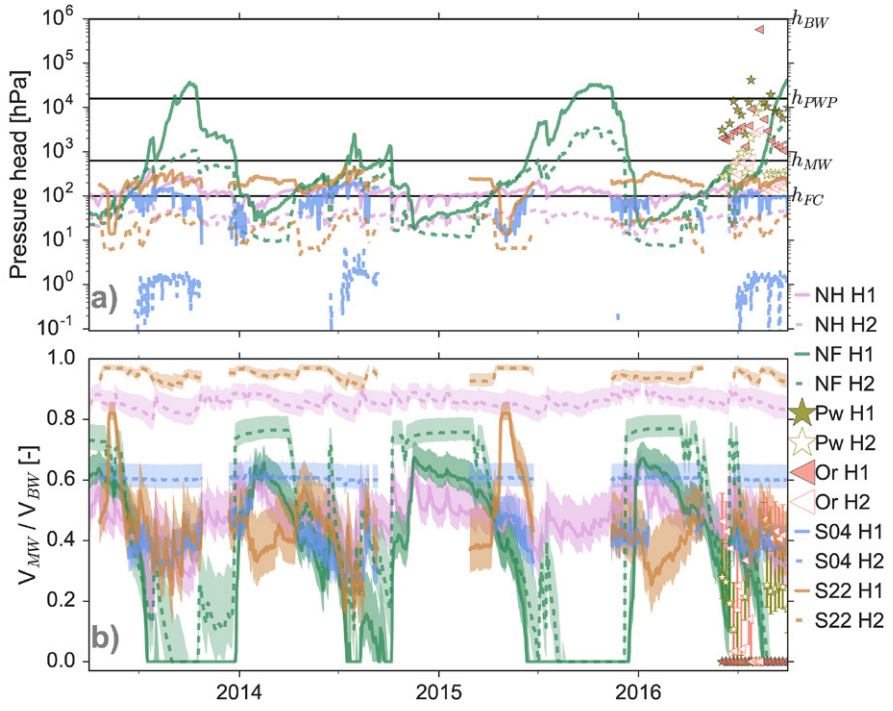

Fig. 5. (a) Soil water pressure head derived from the time series of measured soil moisture at 10 cm (H1) and in the second horizon (H2) using the water retention curve for each site as shown in Fig. 1. Horizontal lines represent pressure heads at field capacity (h_{FC}), the limit of mobile water (h_{MW}), the permanent wilting point (h_{PWP}), and the limit of bulk water analysis (h_{BW}); and (b) the ratio between water volume extractable by suction lysimeter (V_{MW}) and water extractable by cryogenic extraction or direct equilibration (V_{BW}) as defined in Eq. [3]. The shaded area represents the variation in V_{BW}/V_{MW} depending on a range of assumed h_{MW} (500–1000 hPa).

at the locations in Bruntland Burn, with a pronounced drying during summer, when the pressure head was usually below field capacity (h_{FC}). Note that the pronounced drying for NF was probably explained by the soil moisture sensor location directly below a dense Scots pine canopy, leading to reduced infiltration due to high interception losses (Soulsby et al., 2017). At Dorset, where weekly measurements were available during summer 2016, the soil's pressure head was between field capacity and the permanent wilting point (h_{PWP}). For Krycklan, the pressure head was close to h_{FC}, with a pronounced wetting of pressure heads below field capacity during snowmelt periods (Fig. 5a).

The variability of soil moisture and the corresponding pressure heads directly affected the soil moisture volumes that potentially could be sampled with suction lysimeters (V_{MW}, Fig. 1). Consequently, the ratio of the mobile to bulk soil water volume (V_{MW}/V_{BW}) varied with time as a function of the pressure head and the shape of the water retention curve. For the soils at Bruntland Burn, MW accounted for about 40 to 65% of the BW at the 10-cm depth during winter and early spring but fell below 40% during summer (Fig. 5b). There were occasions during the exceptionally dry summer of 2013 (~10-yr return period) when the suction lysimeters were not able to extract any water. The problem of available water for the suction lysimeter was more pronounced for the Dorset sites, where lysimeters could not extract water at about 80% of the overall sampling locations and occasions. The infrequency of MW in the upper soil is supported by the V_{MW}/V_{BW} ratio that indicates that no MW was present during the summer of 2016 at Dorset. For Krycklan, the fraction of MW at the 10-cm soil depth was highly responsive to precipitation and evaporative changes and dropped below 30% on a few occasions. However, in the second horizon, the MW fraction was generally high (>60%) and showed little variation with time. The general pattern of the variability in V_{MW}/V_{BW} is persistently independent of the pressure head applied by the suction lysimeter, as shown for the range of pressure heads between 500 and 1000 cm in Fig. 5b.

Simulation of Soil Moisture

The model differentiation into either a one-pore (OPD) or two-pore domain (TPD) did not affect the soil hydraulics simulations (Fig. 6d, 7d, and 8d). Simulated soil moisture was usually close to the observed soil moisture, with MAE values between 0.02 and 0.11 cm^3 cm^{-3} for most sites (Supplemental Table S1). At NF, the MAE was 0.11 cm^3 cm^{-3} because soil drying during the growing season was underestimated in the simulations compared with the observations. However, as discussed above, we relate the pronounced drying as observed at NF to the location of the soil moisture sensor beneath a dense canopy. Soil moisture at S04 was underestimated in the simulations, which led to a MAE of 0.21 cm^3 cm^{-3}. However, soil moisture dynamics at S04, with little variation during the winter and relatively little response to precipitation inputs, were relatively well met ($r = 0.79$ at 10 cm and $r = 0.66$ at 50 cm, $p < 0.01$).

Simulation of Soil Water Isotopes

Simulations of the soil water isotopes were usually improved when using a TPD rather than OPD (Fig. 9). The OPD approach usually overestimated the isotopic fractionation (brown curves in Fig. 6b, 7b, and 8b), which led to MAEs between observed and simulated BW δ^2H at the 10-cm depth between 5 and 15‰. The TPD simulations resulted in lower MAEs of BW δ^2H of 3.7 to 6.7‰, approaching or reaching the observed standard deviation in the

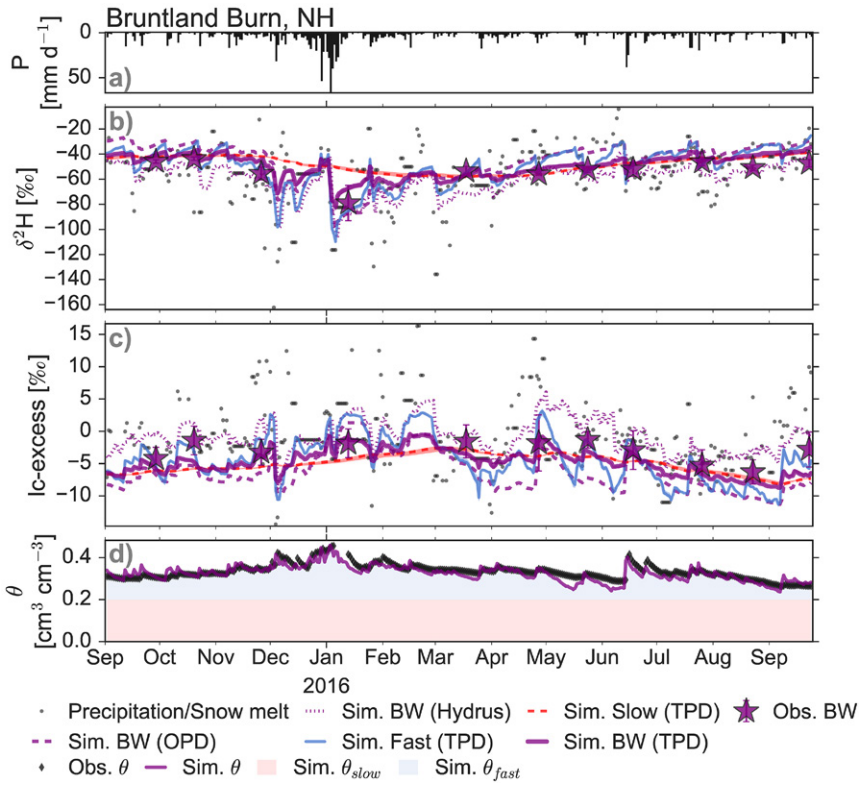

Fig. 6. Observed (Obs.) and simulated (Sim.) soil water isotope and moisture dynamics at the NH site at Bruntland Burn for the period of bulk soil water sampling (2015–2016): (a) precipitation and snowmelt input; (b) δ^2H and (c) line-conditioned excess (lc-excess) dynamics of the bulk soil water, with measurements as stars and simulation as purple lines (solid lines for the two-pore domain [TPD], dashed line for the one-pore domain [OPD], and dotted line for HYDRUS). Also shown are simulated isotopic composition (in b and c) and soil moisture θ (in d) of fast (blue) and slow (red) domains from the TPD simulations. Shaded areas in (b) and (c) represent the variability in simulated fast, simulated slow, and simulated bulk soil water (BW) for the range of assumed mobile water pressure head h_{MW} of 500 to 1000 hPa.

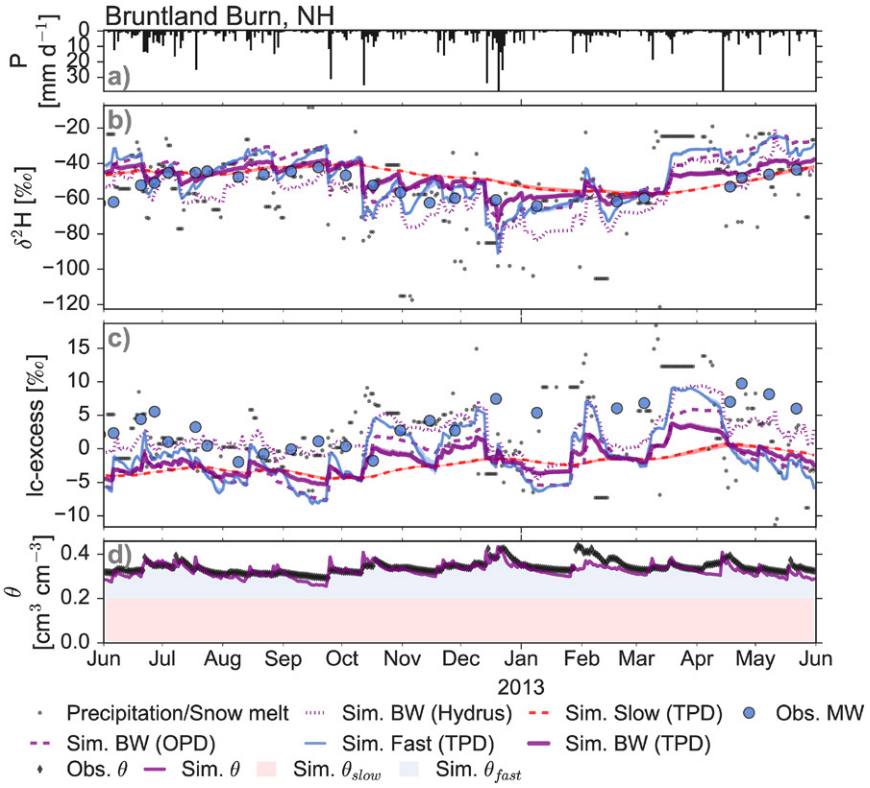

Fig. 7. Observed (Obs.) and simulated (Sim.) soil water isotope and moisture dynamics at the NH site at Bruntland Burn for the period of mobile soil water sampling (2011–2013): (a) precipitation and snowmelt input; (b) δ^2H and (c) line-conditioned excess (lc-excess) dynamics of mobile soil water, with measurements as points and simulation of bulk soil water isotopes as purple lines (solid lines for the two-pore domain [TPD], dashed line for the one-pore domain [OPD], and dotted line for HYDRUS). Also shown are simulated isotopic composition (in b and c) and soil moisture θ (in d) of fast (blue) and slow (red) domains from the TPD simulations. Shaded areas in (b) and (c) represent the variability in simulated fast, simulated slow, and simulated bulk soil water (BW) for the range of assumed mobile water pressure head h_{MW} of 500 to 1000 hPa.

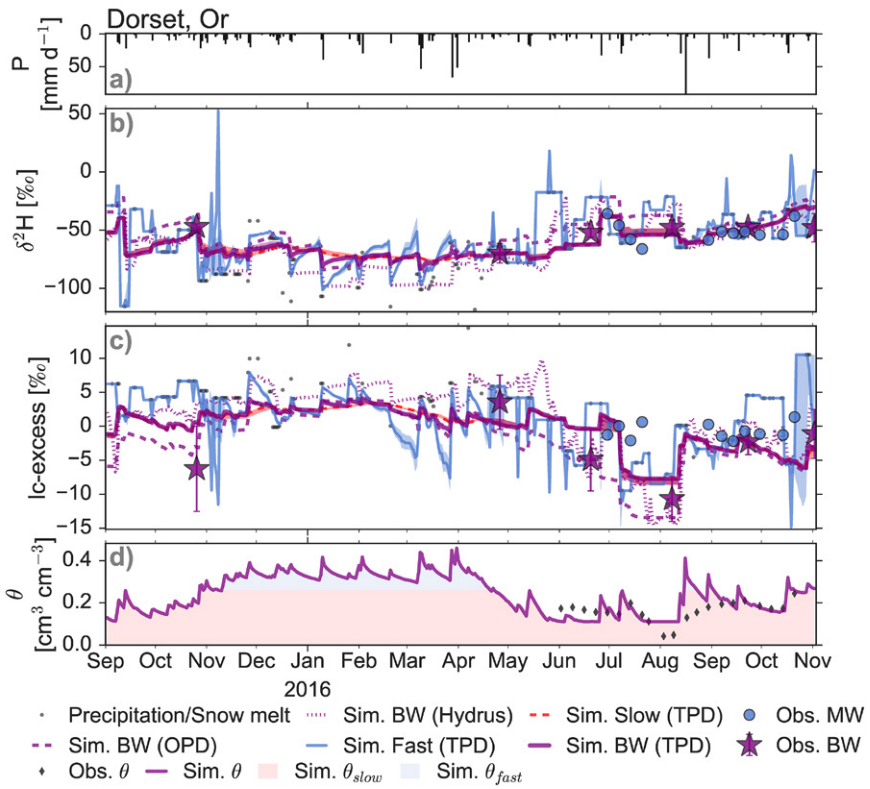

Fig. 8. Observed (Obs.) and simulated (Sim.) soil water isotope and moisture dynamics at the Or site at Dorset: (a) precipitation and snowmelt input; (b) δ^2H and (c) line-conditioned excess (lc-excess) dynamics of bulk soil water, with measurements as stars and simulation as purple lines (solid lines for the two-pore domain [TPD], dashed line for the one-pore domain [OPD], and dotted line for HYDRUS). Also shown are observed mobile water isotopes and simulated isotopic composition (in b and c) and the soil moisture θ (in d) of fast (blue) and slow (red) domains from the TPD simulations. Shaded areas in (b) and (c) represent the variability in simulated fast, simulated slow, and simulated bulk soil water (BW) for the range of assumed mobile water pressure head h_{MW} of 500 to 1000 hPa.

field (Fig. 9). The fit between simulated and observed BW lc-excess was also better with the TPD than with the OPD at Bruntland Burn. However, for Dorset and Krycklan, there were only small differences between the simulated fractionation signal in the BW using either OPD or TPD. Simulations of BW δ^2H without isotopic exchange (TPD_noex) were in many cases better than the simulations with OPD but not as good as the TPD simulations. In terms of BW lc-excess, the differences were less pronounced (Fig. 9). The model results for BW δ^2H with HYDRUS-1D were close to the standard deviation observed in the field, but the simulated lc-excess values showed higher deviations for the HYDRUS-1D results than for the SWIS simulations (Fig. 9).

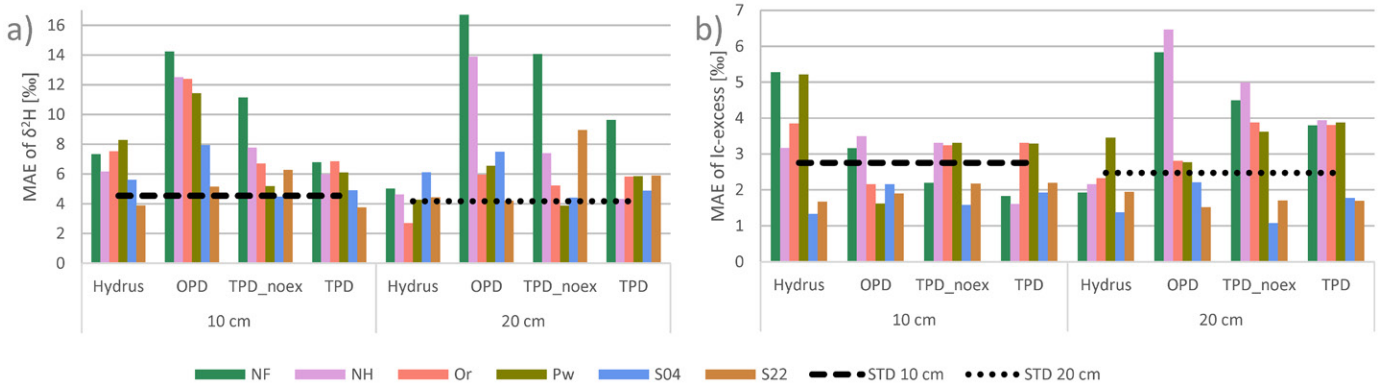

Fig. 9. Comparison of the mean absolute error (MAE) between observed and simulated (a) δ^2H and (b) line-conditioned excess (lc-excess) of bulk water simulated with HYDRUS-1D or the SWIS model using the one-pore domain (OPD) or the two-pore domain without (TPD_noex) or with (TPD) isotopic exchange via water vapor. The dashed and dotted lines show the average standard deviations for a sampling campaign at the individual sites.

The MAE between observed and simulated δ^2H or lc-excess was usually higher for the simulation of the MW than the BW. Simulating the TPD with exchange via water vapor did not improve the simulations of MW isotopic compositions, but the HYDRUS-1D results matched best (Supplemental Table S1).

Dual-isotope plots including a bivariate kernel density distribution underline the improved goodness-of-fit for TPD compared with OPD and illustrate that the simulations with the TPD approach lay within or close to the probable distribution of the isotopic compositions present in the field for most days (Supplemental Fig. S4).

Regarding the BW lc-excess dynamics, we observed that the lc-excess signal did not linearly follow the seasonal increase and decrease in PET at Bruntland Burn. Instead, the BW lc-excess stayed close to zero during spring, while PET increased and the BW-lc excess decreased considerably only during high PET rates. The BW lc-excess stayed negative at the end of the summer, despite decreasing PET rates and increased only slowly during autumn. This led to a hysteresis effect, and the lag response of the BW lc-excess to PET was interpreted as an indication of a two-pore domain (Sprenger et al., 2017b). Our simulations support this interpretation because neither the HYDRUS-1D nor the OPD approach or TPD_noex could simulate the hysteresis pattern (Fig. 10e–10g), while the simulation with the TPD resulted in a lagged response of BW lc-excess to PET (Fig. 10h).

Discussion

Why Mobile and Bulk Soil Water Isotope Compositions Differ

A potential explanation for the observed differences between MW and BW isotopic composition is the different pore spaces that can be effectively sampled using the two methods applied in this study. Detection of an evaporation signal in BW but not in MW is consistent with other studies that sampled both δ_{BW} and δ_{MW} in different environments (Brooks et al., 2009; Goldsmith et al., 2012). However, in contrast to studies of clayey soils by Araguás-Araguás et al. (1995), Figueroa-Johnson et al. (2007), Brooks et al. (2009), and Oshun et al. (2016), we did not see in our low-clay-content soils that the MW was generally more enriched in heavy

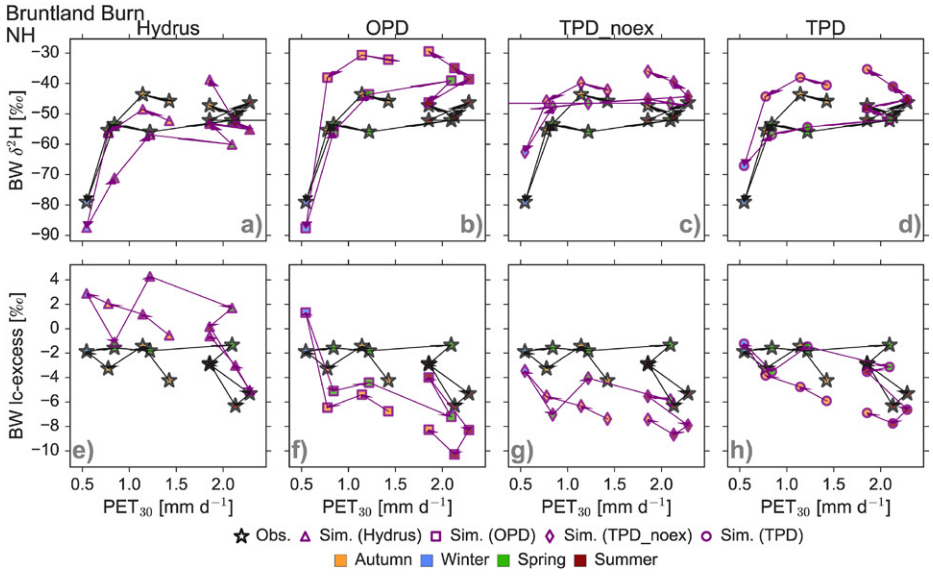

Fig. 10. Observations (stars) and simulations of the relationship between the average potential evapotranspiration (PET) during the 30 d prior to the sampling (PET_{30}) and (a–d) the bulk soil water (BW) δ^2H and (e–h) the BW line-conditioned excess (lc-excess) for the NH site at Bruntland Burn: simulations with (a,e) HYDRUS-1D; (b,f) the one-pore domain (OPD), (c,g) the two-pore domain approach without isotopic exchange via vapor (TPD_noex); and (d,h) the two-pore domain with isotopic exchange (TPD). Colors of the marker fillings indicate the meteorological seasons.

isotopes than the BW. This can probably be related to recent findings showing that waters in the slow flow domain interact with mineral surfaces, changing the isotopic compositions accordingly (Oerter et al., 2014; Gaj et al., 2017; Newberry et al., 2017). This would be stronger the higher the clay content. However, at our sites, MW was on average more depleted than BW (Fig. 3a and 4), and the isotopic variability of infiltrating water influenced the soil water isotopic composition much more strongly than potential interactions with clay minerals.

For the Dorset locations, where BW and MW samples were both taken during summer 2016, δ_{MW} responded to δ_P input, while δ_{BW} remained relatively stable. Thus, it seems that the relationship between MW and BW isotopic compositions is variable with time and there is no general δ-offset between the soil waters held in different pore spaces. Landon et al. (1999) reported that samples from suction lysimeters were more depleted in $\delta^{18}O$ after snowmelt (infiltration of $\delta^{18}O$-depleted water) than BW extracted from soil cores with azeotropic distillation (Revesz and Woods, 1990) for a sandy soil (clay content <8%). These observations are similar to our findings for the Krycklan site S22, where δ_{MW} and δ_{BW} did not generally differ after snowmelt. Parallel soil water isotope sampling with cryogenic extraction and other methods during summer revealed in other studies that BW was more depleted than more mobile water and could therefore result from infiltration weeks or months prior to the sampling (e.g., due to depleted winter precipitation) (Geris et al., 2015a; Sprenger et al., 2015a; Oerter and Bowen, 2017). However, recently published issues with cryogenic extraction could also be partly responsible for these observations, as discussed by Orlowski et al. (2016). Parallel sampling of MW and BW in the study of Zhao et al. (2013) also did not reveal a constant offset between δ_{MW} and δ_{BW} in a loamy soil. Instead, BW tended to be more enriched than MW with declining soil moisture (Zhao et al., 2013), which we also observed for the Dorset locations (Or and Pw) and S22. Thus, while our study was limited to northern environments, we see many parallels with studies conducted in Mediterranean (Brooks et al., 2009; Goldsmith et al., 2012) or subtropical (Zhao et al., 2013) climates in terms of differences between the evaporative enrichment in BW compared with MW. Our results suggest that the age of waters held in different pore spaces can explain the isotopic differences between MW and BW. While MW consists of relatively young water that percolates more quickly through the soil, BW can be composed of water of various ages. The "older" that water in the top 10 cm becomes, the more likely that the pore water experienced evaporation losses and therefore shows an isotopic fractionation signal.

The Relevance of Relative Volumes for Interpretation of Soil Water Isotope Data

Beside the hydro-meteorological forcing that determines the interplay of evaporative enrichment and input of meteoric water (Sprenger et al., 2017c), the soil physical characteristics determining the water retention and thus the volume of mobile (V_{MW}) and bulk water (V_{BW}) are of great relevance for the isotopic differences between MW and BW. For example, the Krycklan sites had the smallest differences between MW and BW lc-excess, which can be related to the high soil moisture values at S04 and high V_{MW}/V_{BW} ratio at S22. These conditions ensure that there was generally substantially more MW present, resulting in relatively faster turnover rates in the topsoil (young water).

The main differences between V_{MW} and V_{BW} were generally observed during the growing season. This has implications when using stable isotopes to infer the root water uptake pattern of plants because the water sampled with suction lysimeters can be a relatively small fraction of the BW. Differences between the isotopic composition of MW and plant water are thus not necessarily paradoxical but rather may be directly related to the water that cannot be sampled with suction lysimeters but is nevertheless available for plant water uptake ($h_{PWP} - h_{MW}$). In this context, we therefore question the conclusion that it is "puzzling why plants would 'prefer' water that is not easiest, energetically, to obtain" (McDonnell, 2014), when based on differences in the isotopic composition of MW and xylem water. In this case, plants are not preferring tightly retained water over mobile water. Berry et al. (2017) presented hypothetical cases where water could either be sampled by suction lysimeter or not and discussed the consequences in light of the TWW hypothesis. We extend this concept by including the V_{MW}/V_{BW} ratio and its time-variant character to emphasize the importance of the different soil water volumes held at different pressure heads, which may or may not be available for sampling or root water uptake. Thus, the timing of isotope sampling at the soil–vegetation interface appears to be crucial and needs to be considered when studying "ecohydrological separation" between soil water and vegetation. This is supported by recent studies by Hervé-Fernández et al. (2016) and McCutcheon et al. (2016), who found that the TWW hypothesis might be temporally limited and not persistent with time. While early studies on the TWW were limited to two or three sampling times (Brooks et al., 2009; Goldsmith et al., 2012), our analysis reveals that the water volumes held in different pore sizes can be highly variable depending on the seasonally variable hydro-meteorological conditions and soil textural composition. In the light of recent findings by Vargas et al. (2017) that there is an isotopic exchange between mobile and tightly retained water, the relative volumes of these two different pore spaces as shown in our study appear to be highly relevant. While this concept of differing soil water volumes sampled with the different methods is applicable for all soil types and climatic conditions, the processes of the interaction between mobile and retained water needs to be better understood. The applied SWIS model provides an adequate tool to assess these interactions via water vapor as discussed in the following.

Distinguishing between Pore Spaces Improves Simulation of Stable Isotopes

Our simulations support the idea that the soil waters held in different pore spaces do not always represent a well-mixed system. In our study, the modeling approach assuming a one-pore domain (OPD) represented well-mixed conditions between

water of different pore sizes. The OPD approach usually showed poorer goodness-of-fit than the two-pore domain (TPD) modeling approach, where the pore space was divided into slow and fast flow domains. Thus, the TPD provided an improved representation of the processes in the vadose zone. This improvement holds true independently from the assumed pressure head applied by the suction lysimeter, defining the differentiation between fast and slow flow domains in the range between 500 and 1000 hPa. While Good et al. (2015) showed that accounting for the hydrologic connectivity between fast and slow flow domains to simulate isotope balances on global scales was necessary, we show the relevance of the isotopic exchange via vapor exchange, which has not been accounted for before in isotope modeling. In contrast to Good et al. (2015), our findings do not indicate that the water in the slow flow domain will not eventually become runoff, since it undergoes vertical movement, although at a slower rate, while its isotopic composition is in exchange with the faster flow domain via vapor exchange.

However, the observed and simulated evaporation-fractionated signal (lc-excess < 0) in the BW at the 10-cm soil depth will not reach the groundwater or stream water because this water subsequently mixes with newly introduced precipitation and snowmelt (with lc-excess ≈ 0‰) as described by Sprenger et al. (2016b). Our simulations depicted the pattern of lc-excess approaching zero with depth (not shown), as observed in soils in temperate to tropical regions (Sprenger et al., 2016b) and also recently presented in data from a northern environment (Sprenger et al., 2017b). Further, groundwater data from the Bruntland Burn and Krycklan showed no signs of evaporative enrichment (Fig. 4), and a detailed spatial analysis in Bruntland Burn revealed that groundwater lc-excess is generally positive (Scheliga et al., 2017). Thus, the modeling results underline that the isotopic difference between topsoil (plotting below the LMWL) and stream and groundwater (plotting on the LMWL) does not necessarily require a division of the subsurface flow into two independent pore domains with no isotopic exchange between the fast and slow flow domains as defined in the TWW hypothesis. Our modeling results further showed that the inferred TWWs are not necessarily independent pore domains that do not interact, because the TPD simulation with no isotopic exchange via vapor exchange (TPD_noex) led to a lower goodness-of-fit than the TPD simulation with isotopic exchange via vapor. Thus, our simulations support the recent experimental evidence by Vargas et al. (2017) that the slow flow soil domain does interact isotopically with mobile waters. Other isotope field studies also showed that a quick component of the subsurface flow did not coincide with the latest precipitation input signal but represented a mixture of event and pre-event water (Dewalle et al., 1988; McDonnell, 1990; Wenner et al., 1991; Anderson et al., 1997; Kelln et al., 2007). Our simulations, which were improved when the MW and BW were in isotopic exchange, provided new insight into what the interaction between the waters of different flow velocities (and thus of different ages) might look like. However, the HYDRUS-1D model that cannot account for evaporative enrichment gave the best match to the MW observations, which did not show evaporative fractionation. Due to the relatively low evaporation rates at the studied sites of the northern latitudes, the mismatch between observations of BW lc-excess and simulations with HYDRUS-1D will therefore be higher in environments with higher evaporative losses.

For the Krycklan site S04, where we generally saw very limited isotopic fractionation, the differences between the modeling approach with (TPD) or without (TPD_noex) isotopic exchange between the two pore domains did not make a major difference in the goodness-of-fit. Additionally, simulations with HYDRUS-1D were not much different from the SWIS results at S04. Because S04 is the wettest sampling location and has the highest organic matter content of our study, our findings indicate that organic matter and the related high soil water content could potentially be of relevance for the exchange between the water held at different pressure heads in the pore space. The other sites experience drying out, which leads to a temporal variability of the V_{MW}/V_{BW} ratio (Fig. 5b). Thus, simulations with the TPD support observations that a phase of drying out enhances the development of two pore domains of different isotopic composition, as seen in a Mediterranean climate by Brooks et al. (2009) that led to the original positing of the TWW hypothesis.

The simulation of the MW isotopic composition was generally less successful than the simulation of the BW because the isotopic fractionation of the MW was overestimated. While we saw very little fractionation in the observed MW isotopic composition, the model results showed high fractionation during dry periods, as for example in April and May 2013 at Bruntland Burn (see in Fig. 7). When the volume of the MW dries out, the kinetic fractionation of the MW becomes increasingly more pronounced, with less water volume remaining in the MW pore space. This mismatch regarding the MW does not stem from an underestimation of the pressure head applied by the suction lysimeter, since the simulation with higher pressure head for suction lysimeters did not improve the model fit (blue shaded area in Fig. 7b and 7c). An explanation could be that the delineation of the subsurface into two pore domains does not reflect the soil physical processes during evaporation as assumed in the model concept of SWIS; instead, a continuum from the largest pores of highest mobility to the smallest pores of lowest mobility would probably be a better representation of the subsurface conditions. However, this would increase model complexity and come at the expense of more parameters, which would be more difficult to define.

Our results from the SWIS simulations are consistent with recent findings by Knighton et al. (2017), who also showed that the MW isotopic composition could not be properly simulated when percolation was assumed to be limited to preferential flow. Instead, a model approach with a partially mixed subsurface gave the best simulations of the observed δ_{MW} dynamics (Knighton et al., 2017). However, the simulations by Knighton et al. (2017) also overestimated the MW isotopic enrichment—independent of their mixing assumptions. Thus, there is a general need to better understand how the different pore spaces are affected by evaporative enrichment in the topsoil water.

The presented simulations suggest that the tightly retained water can contain isotopically enriched water from the previous summer, while the more mobile water responds to recent precipitation inputs (see Winter 2015–2016 in Fig. 6). Because the older water dominates the smaller pores, the response of the BW lc-excess lags the dynamics of the evaporation losses, leading to hysteresis loops that could only be well simulated when considering a TPD (Fig. 10). Our simulations for Bruntland Burn, therefore, support the initial interpretation by Sprenger et al. (2017b) of the observed relationship between BW lc-excess and evaporation losses: that "old" water in smaller pore spaces leads to a memory effect (hysteresis loops). This would also be in agreement with other field studies (Geris et al., 2015a; Sprenger et al., 2015a; Oerter and Bowen, 2017), where a memory effect of older water was suggested as discussed above.

Hence, the findings of our simulations impact travel time estimates for the unsaturated zone because soil water isotope data sampled with suction lysimeters are often used in travel time studies (Asano et al., 2002; Muñoz-Villers and McDonnell, 2012; Tetzlaff et al., 2014). Such travel time analyses, based on suction lysimeter data (see list of studies in Sprenger et al., 2016b), will then be limited to the mobile waters and thus underestimate travel times through the unsaturated zone. To our knowledge, this difference has not been discussed or even noted in travel time studies. More recently, BW data were used for travel time estimates of the unsaturated zone (Sprenger et al., 2016c, 2016a), which accounts—according to our findings—for the entire pore space including the fast and slow flow domains.

Our results for the three different northern catchments suggest that interaction between the different pore spaces varies depending on the soil properties (i.e., water retention characteristics) and the soil water content. However, it needs to be tested whether this is equally applicable for different environments. Our conceptualization of a two-pore domain is obviously a simplification of a more continuous system of waters with highly variable mobilities across the pore space. However, the relationship between BW lc-excess and evaporation losses presented here provides new insights into an appropriate and reasonable model representation of the relevant hydrological processes.

Conclusion

We first showed measured differences in the isotopic composition of MW (sampled with suction lysimeters) and BW (sampled with the direct-equilibration method) in soils of northern environments. The MW isotopic compositions plotted on the LMWL (input signal), while the BW isotopes plotted below the LMWL (isotopic enrichment) in the dual-isotope space, which agrees with observations in warmer climatic regions made by others. These differences in lc-excess show opportunities to study the activation of preferential flow paths and interactions between macropores and the soil matrix. We suggest that the ratio between the volumes of the two soil water pools, here assessed as V_{MW}/V_{BW}, is relevant to the observed differences in stable isotopes of the two pore domains. Thus, MW and BW isotopes are likely to be more different the drier the soil becomes—as seen in the field measurements. This has direct implications for the interpretation of the soil water isotope composition data, when relating them to plant water isotope measurements to infer root water uptake patterns or when estimating transit or residence time distribution in soils. Importantly, we conclude that, under dry conditions when the mobile water is a relatively small fraction of the BW, an isotopic composition of the plant water similar to that of the BW is not paradoxical. We underlined our conclusion with simulations, which showed that ignoring the evaporative enrichment such as in HYDRUS-1D leads to an underestimation of deuterium and oxygen values in the topsoil. While this underestimation is relatively moderate in the low-energy environments studied here, the effect is likely to be more intense in regions with higher evaporative losses. When including evaporative enrichment in the simulations, assuming a uniform pore space (one-pore domain) leads to an overestimation of the fractionation signal in the topsoil. Accounting for two different pore spaces, divided into fast and slow flow (TPD), improved the simulations and could reflect the observation that BW lc-excess does not necessarily relate linearly to soil evaporation losses. Because the TPD approach with isotopic exchange via water vapor was closer to the observed isotope pattern than a conceptualization without exchange via vapor, we conclude that the mobile and tightly retained waters in the subsurface interact and are not independent water pools. How intense this exchange between the two pore domains is and whether all water of the slow flow domain takes part in the exchange needs further investigation. However, our measured and simulated data indicate that the age of water at the pore scale has a major influence on the evaporation signal of the soil water, with younger mobile water being very similar to the input signal but water of the slow flow domain showing isotopic fractionation due to soil evaporation.

Variables

A	area of the surface for liquid–vapor exchange, differentiated between the fast and slow flow domains (A_f and A_s, respectively), cm
α	air-entry value (van Genuchten parameter), cm^{-1}
BW	bulk soil water, sampled with cryogenic extraction or direct equilibration method
C	atomic ratios for ^2H and ^{18}O, differentiated between C_{fast} and C_{slow}, %
C_{eq}	equilibrium concentration between two water pools, %
DDF	degree day factor, mm d^{-1} $°C^{-1}$
δ_{BW}	isotopic composition (δ^2H and/or $\delta^{18}O$) of bulk soil water, ‰
δ_{MW}	isotopic composition (δ^2H and/or $\delta^{18}O$) of mobile soil water, ‰
δ_P	isotopic composition (δ^2H and/or $\delta^{18}O$) of precipitation and snowmelt input, ‰
e_w	saturated vapor pressure, hPa
f_a	areal factor that scales the surface area of the liquid–vapor interface
GMWL	global meteoric water line
h_{BW}	pressure head limit of bulk water sampled with the direct-equilibration method, hPa
h_{FC}	pressure head of field capacity, hPa
h_f	pressure head in the fast flow domain, hPa

h_{MW}	pressure head limit of mobile water sampled with suction lysimeters, hPa
h_{PWP}	pressure head of the permanent wilting point, hPa
h_s	pressure head in the slow flow domain, hPa
K	hydraulic conductivity, cm d^{-1}
k	parameter for the exchange via water vapor phase, cm hPa^{-1} d^{-1}
lc-excess	line-conditioned excess, ‰
λ	dispersivity parameter, cm
LMWL	local meteoric water line
MAE	mean absolute error
MW	mobile soil water, sampled with suction lysimeter
n	shape parameter (van Genuchten parameter)
OPD	one-pore domain
T	mean daily air temperature, °C
TPD	two-pore domain with isotopic exchange via vapor exchange
TPD_noex	two-pore domain without isotopic exchange via vapor exchange
θ	volumetric water content, cm^3 cm^{-3}
θ_r	residual volumetric water content, cm^3 cm^{-3}
θ_s	saturated volumetric water content, cm^3 cm^{-3}
p	significance level
PET_{30}	30-day running mean of potential evapotranspiration, mm d^{-1}
P_1, P_{30}	weighted running average (1 and 30 d) isotopic composition of the precipitation and snowmelt input as in δ^2H P_1 and lc-excess P_1 and δ^2H P_{30} and lc-excess P_{30}, respectively, ‰
ϕ	soil porosity (with ϕ_f and ϕ_s for the fast and slow domains, respectively)
r	Pearson's correlation coefficient
r_f	radius of the fast flow domain, cm
r_s	radius of the slow flow domain, cm
ρ_w	water density, g cm^{-3}
SM	snowmelt, mm
S	packing parameter for the surface area model ($S = 0.15$)
SWE	snow water equivalent, mm
σ	surface tension, J m^{-2}
V_{BW}	bulk soil water volume that can be sampled with the direct-equilibration method, mm
V_f	soil water volume in the fast flow domain, mm
V_{MW}	mobile (of the fast flow domain) soil water volume that can be sampled with suction lysimeters, mm

Acknowledgments

We thank Audrey Innes for support with the isotope analysis at University of Aberdeen for the Bruntland Burn and Krycklan sites, Johannes Tiwari (SLU) for the isotope sampling in Krycklan, Pernilla Löfvenius (SLU) for providing PET data for Krycklan, Pertti Ala-aho for providing snowmelt simulations for Krycklan, and Kimberely Janzen (University of Saskatoon) for soil water isotope analysis for the Dorset sites. The work at Krycklan was supported by KAW Branch-Points. We thank the European Research Council (ERC, project GA 335910 VeWa) for funding. We thank two anonymous reviewers and the associate editor for their suggestions and comments.

References

Ala-aho, P., D. Tetzlaff, J.P. McNamara, H. Laudon, P. Kormos, and C. Soulsby. 2017a. Modeling the isotopic evolution of snowpack and snowmelt: Testing a spatially distributed parsimonious approach. Water Resour. Res. 53:5813–5830. doi:10.1002/2017WR020650

Ala-aho, P., D. Tetzlaff, J.P. McNamara, H. Laudon, and C. Soulsby. 2017b. Using isotopes to constrain water flux and age estimates in snow-influenced catchments using the STARR (Spatially distributed Tracer-Aided Rainfall–Runoff) model. Hydrol. Earth Syst. Sci. 21:5089–5110. doi:10.5194/hess-21-5089-2017

Allen, R.G., L.S. Pereira, D. Raes, and M. Smith. 1998. Crop evapotranspiration: Guidelines for computing crop water requirements. Irrig. Drain. Pap. 56. FAO, Rome.

Anderson, S.P., W.E. Dietrich, R. Torres, D.R. Montgomery, and K. Loague. 1997. Concentration–discharge relationships in runoff from a steep, unchanneled catchment. Water Resour. Res. 33:211–225. doi:10.1029/96WR02715

Araguás-Araguás, L., K. Rozanski, R. Gonfiantini, and D. Louvat. 1995. Isotope effects accompanying vacuum extraction of soil water for stable isotope analyses. J. Hydrol. 168:159–171. doi:10.1016/0022-1694(94)02636-P

Asano, Y., T. Uchida, and N. Ohte. 2002. Residence times and flow paths of water in steep unchannelled catchments, Tanakami, Japan. J. Hydrol. 261:173–192. doi:10.1016/S0022-1694(02)00005-7

Barnes, C., and G. Allison. 1983. The distribution of deuterium and ^{18}O in dry soils: 1. Theory. J. Hydrol. 60:141–156. doi:10.1016/0022-1694(83)90018-5

Berry, Z.C., J. Evaristo, G. Moore, M. Poca, K. Steppe, L. Verrot, et al. 2017. The two water worlds hypothesis: Addressing multiple working hypotheses and proposing a way forward. Ecohydrology 2017:e1843. doi:10.1002/eco.1843

Beven, K., and P. Germann. 2013. Macropores and water flow in soils revisited. Water Resour. Res. 49:3071–3092. doi:10.1002/wrcr.20156

Birkel, C., C. Soulsby, and D. Tetzlaff. 2014. Developing a consistent process-based conceptualization of catchment functioning using measurements of internal state variables. Water Resour. Res. 50:3481–3501. doi:10.1002/2013WR014925

Blume-Werry, G., J. Kreyling, H. Laudon, A. Milbau, and F. Gilliam. 2016. Short-term climate change manipulation effects do not scale up to long-term legacies: Effects of an absent snow cover on boreal forest plants. J. Ecol. 104:1638–1648. doi:10.1111/1365-2745.12636

Brooks, J.R., H.R. Barnard, R. Coulombe, and J.J. McDonnell. 2009. Ecohydrologic separation of water between trees and streams in a Mediterranean climate. Nat. Geosci. 3:100–104. doi:10.1038/ngeo722

Buttle, J.M., and M.C. Eimers. 2009. Scaling and physiographic controls on streamflow behaviour on the Precambrian Shield, south-central Ontario. J. Hydrol. 374:360–372. doi:10.1016/j.jhydrol.2009.06.036

Calder, I.R. 1986. The influence of land use on water yield in upland areas of the U.K. J. Hydrol. 88:201–211. doi:10.1016/0022-1694(86)90091-0

Campbell, G.S. 1985. Water potential. In: G.S. Campbell, editor, Soil physics with Basic: Transport models for soil–plant systems. Dev. Soil Sci. 14. Elsevier, Amsterdam. p. 40–48.

Chai, T., and R.R. Draxler. 2014. Root mean square error (RMSE) or mean absolute error (MAE)? Arguments against avoiding RMSE in the literature. Geosci. Model Dev. 7:1247–1250. doi:10.5194/gmd-7-1247-2014

Criss, R.E. 1999. Principles of stable isotope distribution. Oxford Univ. Press, New York.

Dansgaard, W. 1964. Stable isotopes in precipitation. Tellus 16:436–468. doi:10.3402/tellusa.v16i4.8993

Dawson, T.E., and J.R. Ehleringer. 1991. Streamside trees that do not use stream water. Nature 350:335–337. doi:10.1038/350335a0

Dewalle, D.R., B.R. Swistock, and W.E. Sharpe. 1988. Three-component tracer model for stormflow on a small Appalachian forested catchment. J. Hydrol. 104:301–310. doi:10.1016/0022-1694(88)90171-0

Eimers, M.C., and P.J. Dillon. 2002. Climate effects on sulphate flux from forested catchments in south-central Ontario. Biogeochemistry 61:337–355. doi:10.1023/A:1020261913618

Figueroa-Johnson, M.A., J.A. Tindall, and M. Friedel. 2007. A comparison of ^{18}Od composition of water extracted from suction lysimeters, centrifugation, and azeotropic distillation. Water Air Soil Pollut. 184:63–75. doi:10.1007/s11270-007-9399-8

Gaj, M., S. Kaufhold, P. Koeniger, M. Beyer, M. Weiler, and T. Himmelsbach. 2017. Mineral mediated isotope fractionation of soil water. Rapid Commun. Mass Spectrom. 31:269–280. doi:10.1002/rcm.7787

Garvelmann, J., C. Külls, and M. Weiler. 2012. A porewater-based stable isotope approach for the investigation of subsurface hydrological processes. Hydrol. Earth Syst. Sci. 16:631–640. doi:10.5194/hess-16-631-2012

Geris, J., D. Tetzlaff, J. McDonnell, J. Anderson, G. Paton, and C. Soulsby. 2015a. Ecohydrological separation in wet, low energy northern environments? A preliminary assessment using different soil water extraction techniques. Hydrol. Processes 29:5139–5152. doi:10.1002/hyp.10603

Geris, J., D. Tetzlaff, J. McDonnell, and C. Soulsby. 2015b. The relative role of soil type and tree cover on water storage and transmission in northern headwater catchments. Hydrol. Processes 29:1844–1860.

doi:10.1002/hyp.10289

Gerke, H.H., and M.Th. van Genuchten. 1993. A dual-porosity model for simulating the preferential movement of water and solutes in structured porous media. Water Resour. Res. 29:305–319. doi:10.1029/92WR02339

Goldsmith, G.R., L.E. Muñoz-Villers, F. Holwerda, J.J. McDonnell, H. Asbjornsen, and T.E. Dawson. 2012. Stable isotopes reveal linkages among ecohydrological processes in a seasonally dry tropical montane cloud forest. Ecohydrology 5:779–790. doi:10.1002/eco.268

Gonfiantini, R. 1986. Environmental isotopes in lake studies. In: P. Fritz and J.C. Fontes, editors, Handbook of environmental isotope geochemistry. Vol. B. The terrestrial environment. Elsevier, Amsterdam. p. 113–168. doi:10.1016/B978-0-444-42225-5.50008-5

Good, S.P., D. Noone, and G. Bowen. 2015. Hydrologic connectivity constrains partitioning of global terrestrial water fluxes. Science 349:175–177. doi:10.1126/science.aaa5931

Gupta, H.V., H. Kling, K.K. Yilmaz, and G.F. Martinez. 2009. Decomposition of the mean squared error and NSE performance criteria: Implications for improving hydrological modelling. J. Hydrol. 377:80–91. doi:10.1016/j.jhydrol.2009.08.003

Haese, B., M. Werner, and G. Lohmann. 2013. Stable water isotopes in the coupled atmosphere–land surface model ECHAM5-JSBACH. Geosci. Model Dev. 6:1463–1480. doi:10.5194/gmd-6-1463-2013

Haria, A.H., and D.J. Price. 2000. Evaporation from Scots pine (*Pinus sylvestris*) following natural re-colonisation of the Cairngorm mountains, Scotland. Hydrol. Earth Syst. Sci. 4:451–461. doi:10.5194/hess-4-451-2000

Haverd, V., and M. Cuntz. 2010. Soil–Litter–Iso: A one-dimensional model for coupled transport of heat, water and stable isotopes in soil with a litter layer and root extraction. J. Hydrol. 388:438–455. doi:10.1016/j.jhydrol.2010.05.029

Hendry, M.J., E. Schmeling, L.I. Wassenaar, S.L. Barbour, and D. Pratt. 2015. Determining the stable isotope composition of pore water from saturated and unsaturated zone core: Improvements to the direct vapour equilibration laser spectrometry method. Hydrol. Earth Syst. Sci. 19:4427–4440. doi:10.5194/hess-19-4427-2015

Hervé-Fernández, P., C. Oyarzún, C. Brumbt, D. Huygens, S. Bodé, N.E.C. Verhoest, and P. Boeckx. 2016. Assessing the "two water worlds" hypothesis and water sources for native and exotic evergreen species in south-central Chile. Hydrol. Processes 30:4227–4241. doi:10.1002/hyp.10984

Hock, R. 2003. Temperature index melt modelling in mountain areas. J. Hydrol. 282:104–115. doi:10.1016/S0022-1694(03)00257-9

Ingraham, N.L., and R.E. Criss. 1998. The effect of vapor pressure on the rate of isotopic exchange between water and water vapor. Chem. Geol. 150:287–292. doi:10.1016/S0009-2541(98)00109-0

Kelln, C., L. Barbour, and C. Qualizza. 2007. Preferential flow in a reclamation cover: Hydrological and geochemical response. J. Geotech. Geoenviron. Eng. 133:1277–1289. doi:10.1061/(ASCE)1090-0241(2007)133:10(1277)

Knighton, J., S.M. Saia, C.K. Morris, J.A. Archiblad, and M.T. Walter. 2017. Ecohydrologic considerations for modeling of stable water isotopes in a small intermittent watershed. Hydrol. Processes 31:2438–2452. doi:10.1002/hyp.11194

Koeniger, P., J.D. Marshall, T. Link, and A. Mulch. 2011. An inexpensive, fast, and reliable method for vacuum extraction of soil and plant water for stable isotope analyses by mass spectrometry. Rapid Commun. Mass Spectrom. 25:3041–3048. doi:10.1002/rcm.5198

Landon, M.K., G.N. Delin, S.C. Komor, and C.P. Regan. 1999. Comparison of the stable-isotopic composition of soil water collected from suction lysimeters, wick samplers, and cores in a sandy unsaturated zone. J. Hydrol. 224:45–54. doi:10.1016/S0022-1694(99)00120-1

Landwehr, J.M., and T.B. Coplen. 2006. Line-conditioned excess: A new method for characterizing stable hydrogen and oxygen isotope ratios in hydrologic systems. In: International Conference on Isotopes in Environmental Studies, Monte-Carlo, Monaco. 25–29 Oct. 2004. IAEA, Vienna. p. 132–135.

Laudon, H., and M. Ottosson Löfvenius. 2016. Adding snow to the picture: Providing complementary winter precipitation data to the Krycklan Catchment Study database. Hydrol. Processes 30:2413–2416. doi:10.1002/hyp.10753

Laudon, H., I. Taberman, A. Ågren, M. Futter, M. Ottosson-Löfvenius, and K. Bishop. 2013. The Krycklan Catchment Study: A flagship infrastructure for hydrology, biogeochemistry, and climate research in the boreal landscape. Water Resour. Res. 49:7154–7158. doi:10.1002/wrcr.20520

Lidman, F., A. Boily, H. Laudon, and S.J. Köhler. 2017. From soil water to surface water: How the riparian zone controls element transport from a boreal forest to a stream. Biogeosciences 14:3001–3014. doi:10.5194/bg-14-3001-2017

Lozano, F.C., W.H. Parton, J.K.H. Lau, and L. Vanderstar. 1987. Physical and chemical properties for the soils at the Southern Biogeochemical Study Site. Consultant's Rep. 18. Dorset Environ. Sci. Ctr., Dorset, ON, Canada.

Majoube, M. 1971. Fractionnement en oxygene-18 et en deuterium entre l'eau et sa vapeur. J. Chim. Phys. 68:1423–1436. doi:10.1051/jcp/1971681423

McCutcheon, R.J., J.P. McNamara, M.J. Kohn, and S.L. Evans. 2016. An evaluation of the ecohydrological separation hypothesis in a semiarid catchment. Hydrol. Processes 31:783–799. doi:10.1002/hyp.11052

McDonnell, J.J. 1990. A rationale for old water discharge through macropores in a steep, humid catchment. Water Resour. Res. 26:2821–2832. doi:10.1029/WR026i011p02821

McDonnell, J.J. 2014. The two water worlds hypothesis: Ecohydrological separation of water between streams and trees? Wiley Interdiscip. Rev.: Water 1:323–329. doi:10.1002/wat2.1027

McDonnell, J.J., and K. Beven. 2014. Debates—The future of hydrological sciences: A (common) path forward? A call to action aimed at understanding velocities, celerities and residence time distributions of the headwater hydrograph. Water Resour. Res. 50:5342–5350. doi:10.1002/2013WR015141

Mueller, M.H., A. Alaoui, C. Kuells, H. Leistert, K. Meusburger, C. Stumpp, et al. 2014. Tracking water pathways in steep hillslopes by $d^{18}O$ depth profiles of soil water. J. Hydrol. 519A:340–352. doi:10.1016/j.jhydrol.2014.07.031

Muñoz-Villers, L.E., and J.J. McDonnell. 2012. Runoff generation in a steep, tropical montane cloud forest catchment on permeable volcanic substrate. Water Resour. Res. 48:W09528. doi:10.1029/2011WR011316

Nash, J.E., and J.V. Sutcliffe. 1970. River flow forecasting through conceptual models: I. A discussion of principles. J. Hydrol. 10:282–290. doi:10.1016/0022-1694(70)90255-6

Neary, A.J., E. Mistry, and L. Vanderstar. 1987. Sulphate relationships in some central Ontario forest soils. Can. J. Soil Sci. 67:341–352. doi:10.4141/cjss87-030

Newberry, S.L., U.E. Prechsl, M. Pace, and A. Kahmen. 2017. Tightly bound soil water introduces isotopic memory effects on mobile and extractable soil water pools. Isot. Environ. Health Stud. 53:368–381. doi:10.1080/10256016.2017.1302446

Nyberg, L., M. Stähli, P.-E. Mellander, and K.H. Bishop. 2001. Soil frost effects on soil water and runoff dynamics along a boreal forest transect: 1. Field investigations. Hydrol. Processes 15:909–926. doi:10.1002/hyp.256

Oerter, E., and G. Bowen. 2017. In situ monitoring of H and O stable isotopes in soil water reveals ecohydrologic dynamics in managed soil systems. Ecohydrology 10:e1841. doi:10.1002/eco.1841

Oerter, E., K. Finstad, J. Schaefer, G.R. Goldsmith, T. Dawson, and R. Amundson. 2014. Oxygen isotope fractionation effects in soil water via interaction with cations (Mg, Ca, K, Na) adsorbed to phyllosilicate clay minerals. J. Hydrol. 515:1–9. doi:10.1016/j.jhydrol.2014.04.029

Or, D., P. Lehmann, E. Shahraeeni, and N. Shokri. 2013. Advances in soil evaporation physics: A review. Vadose Zone J. 12(4). doi:10.2136/vzj2012.0163

Orlowski, N., L. Breuer, and J.J. McDonnell. 2016. Critical issues with cryogenic extraction of soil water for stable isotope analysis. Ecohydrology 9:1–5. doi:10.1002/eco.1722

Orlowski, N., H.-G. Frede, N. Brüggemann, and L. Breuer. 2013. Validation and application of a cryogenic vacuum extraction system for soil and plant water extraction for isotope analysis. J. Sens. Sens. Syst. 2:179–193. doi:10.5194/jsss-2-179-2013

Oshun, J., W.E. Dietrich, T.E. Dawson, and I. Fung. 2016. Dynamic, structured heterogeneity of water isotopes inside hillslopes. Water Resour. Res. 52:164–189. doi:10.1002/2015WR017485

Peralta-Tapia, A., R.A. Sponseller, D. Tetzlaff, C. Soulsby, and H. Laudon. 2015. Connecting precipitation inputs and soil flow pathways to stream water in contrasting boreal catchments. Hydrol. Processes 29:3546–3555. doi:10.1002/hyp.10300

Revesz, K., and P.H. Woods. 1990. A method to extract soil water for stable isotope analysis. J. Hydrol. 115:397–406. doi:10.1016/0022-1694(90)90217-L

Ritchie, J.T. 1972. Model for predicting evaporation from a row crop with incomplete cover. Water Resour. Res. 8:1204–1213. doi:10.1029/WR008i005p01204

Rothfuss, Y., and M. Javaux. 2017. Reviews and syntheses: Isotopic approaches to quantify root water uptake: A review and comparison of methods. Biogeosciences 14:2199–2224. doi:10.5194/bg-14-2199-2017

Rothfuss, Y., H. Vereecken, and N. Brüggemann. 2013. Monitoring water stable isotopic composition in soils using gas-permeable tubing and infrared laser absorption spectroscopy. Water Resour. Res. 49:3747–3755. doi:10.1002/wrcr.20311

Schaap, M.G., F.J. Leij, and M.Th. van Genuchten. 2001. ROSETTA: A computer program for estimating soil hydraulic parameters with hierarchical pedotransfer functions. J. Hydrol. 251:163–176. doi:10.1016/S0022-1694(01)00466-8

Scheliga, B., D. Tetzlaff, G. Nuetzmann, and C. Soulsby. 2017. Groundwater isoscapes in a montane headwater catchment show dominance of well-mixed storage. Hydrol. Processes 31:3504–3519. doi:10.1002/hyp.11271

Soulsby, C., C. Birkel, J. Geris, J. Dick, C. Tunaley, and D. Tetzlaff. 2015. Stream water age distributions controlled by storage dynamics and nonlinear hydrologic connectivity: Modeling with high-resolution isotope data. Water Resour. Res. 51:7759–7776. doi:10.1002/2015WR017888

Soulsby, C., H. Braun, M. Sprenger, M. Weiler, and D. Tetzlaff. 2017. Influence of forest and shrub canopies on precipitation partitioning and isotopic signatures. Hydrol. Processes 31:4282–4296. doi:10.1002/hyp.11351

Sprenger, M., M. Erhardt, M. Riedel, and M. Weiler. 2016a. Historical tracking of nitrate in contrasting vineyards using water isotopes and nitrate depth profiles. Agric. Ecosyst. Environ. 222:185–192. doi:10.1016/j.agee.2016.02.014.

Sprenger, M., B. Herbstritt, and M. Weiler. 2015a. Established methods and new opportunities for pore water stable isotope analysis. Hydrol. Processes 29:5174–5192. doi:10.1002/hyp.10643

Sprenger, M., H. Leistert, K. Gimbel, and M. Weiler. 2016b. Illuminating hydrological processes at the soil–vegetation–atmosphere interface with water stable isotopes. Rev. Geophys. 54:674–704. doi:10.1002/2015RG000515

Sprenger, M., S. Seeger, T. Blume, and M. Weiler. 2016c. Travel times in the vadose zone: Variability in space and time. Water Resour. Res. 52:5727–5754. doi:10.1002/2015WR018077

Sprenger, M., D. Tetzlaff, and C. Soulsby. 2017a. No influence of CO_2 on stable isotope analyses of soil waters with OA-ICOS. Rapid Commun. Mass Spectrom. 31:430–436. doi:10.1002/rcm.7815

Sprenger, M., D. Tetzlaff, and C. Soulsby. 2017b. Soil water stable isotopes reveal evaporation dynamics at the soil–plant–atmosphere interface of the critical zone. Hydrol. Earth Syst. Sci. 21:3839–3858. doi:10.5194/hess-21-3839-2017

Sprenger, M., D. Tetzlaff, C. Tunaley, J. Dick, and C. Soulsby. 2017c. Evaporation fractionation in a peatland drainage network affects stream water isotope composition. Water Resour. Res. 53:851–866. doi:10.1002/2016WR019258

Sprenger, M., T.H.M. Volkmann, T. Blume, and M. Weiler. 2015b. Estimating flow and transport parameters in the unsaturated zone with pore water stable isotopes. Hydrol. Earth Syst. Sci. 19:2617–2635. doi:10.5194/hess-19-2617-2015

Stähli, M., L. Nyberg, P.-E. Mellander, P.-E. Jansson, and K.H. Bishop. 2001. Soil frost effects on soil water and runoff dynamics along a boreal transect: 2. Simulations. Hydrol. Processes 15:927–941. doi:10.1002/hyp.232

Stumpp, C., P. Maloszewski, W. Stichler, and S. Maciejewski. 2007. Quantification of the heterogeneity of the unsaturated zone based on environmental deuterium observed in lysimeter experiments. Hydrol. Sci. J. 52:748–762. doi:10.1623/hysj.52.4.748

Stumpp, C., W. Stichler, M. Kandolf, and J. Šimůnek. 2012. Effects of land cover and fertilization method on water flow and solute transport in five lysimeters: A long-term study using stable water isotopes. Vadose Zone J. 11(1). doi:10.2136/vzj2011.0075.

Tetzlaff, D., C. Birkel, J. Dick, J. Geris, and C. Soulsby. 2014. Storage dynamics in hydropedological units control hillslope connectivity, runoff generation and the evolution of catchment transit time distributions. Water Resour. Res. 50:969–985. doi:10.1002/2013WR014147

Tetzlaff, D., J. Buttle, S.K. Carey, M.H.J. van Huijgevoort, H. Laudon, J. McNamara, et al. 2015. A preliminary assessment of water partitioning and ecohydrological coupling in northern headwaters using stable isotopes and conceptual runoff models. Hydrol. Processes 29:5153–5173. doi:10.1002/hyp.10515

Vanderborght, J., and H. Vereecken. 2007. Review of dispersivities for transport modeling in soils. Vadose Zone J. 6:29–52. doi:10.2136/vzj2006.0096

van Genuchten, M.Th. 1980. A closed-form equation for predicting the hydraulic conductivity of unsaturated soils. Soil Sci. Soc. Am. J. 44:892–898. doi:10.2136/sssaj1980.03615995004400050002x

van Genuchten, M.Th., F.J. Leij, and S.R. Yates. 1991. The RETC code for quantifying the hydraulic functions of unsaturated soils. EPA/600/2-91/065. USEPA Robert S. Kerr Environ. Res. Lab., Ada, OK.

Vargas, A.I., B. Schaffer, L. Yuhong, and L.S.L. Sternberg. 2017. Testing plant use of mobile vs immobile soil water sources using stable isotope experiments. New Phytol. 215:582–594. doi:10.1111/nph.14616

Volkmann, T.H.M., K. Haberer, A. Gessler, and M. Weiler. 2016. High-resolution isotope measurements resolve rapid ecohydrological dynamics at the soil–plant interface. New Phytol. 210:839–849. doi:10.1111/nph.13868

Volkmann, T.H.M., and M. Weiler. 2014. Continual in situ monitoring of pore water stable isotopes in the subsurface. Hydrol. Earth Syst. Sci. 18:1819–1833. doi:10.5194/hess-18-1819-2014

Wang, H., D. Tetzlaff, and C. Soulsby. 2017a. Assessing the environmental controls on Scots pine transpiration and the implications for water partitioning in a boreal headwater catchment. Agric. For. Meteorol. 240–241:58–66. doi:10.1016/j.agrformet.2017.04.002

Wang, H., D. Tetzlaff, and C. Soulsby. 2017b. Testing the maximum entropy production approach for estimating evapotranspiration from closed canopy shrubland in a low-energy humid environment. Hydrol. Processes 31:4613–4621. doi:10.1002/hyp.11363

Warneck, P., and J.M.J. Williams. 2012. The atmospheric chemist's companion: Numerical data for use in the atmospheric sciences. Springer, Dordrecht, the Netherlands. doi:10.1007/978-94-007-2275-0

Wassenaar, L., M. Hendry, V. Chostner, and G. Lis. 2008. High resolution pore water d^2H and $d^{18}O$ measurements by H_2O (liquid)–H_2O (vapor) equilibration laser spectroscopy. Environ. Sci. Technol. 42:9262–9267. doi:10.1021/es802065s

Weiss, M., and F. Baret. 2014. CAN-EYE output variables: Definitions and theoretical background. INRA, Avignon, France.

Wenner, D., P. Ketcham, and J. Dowd. 1991. Stable isotopic composition of waters in a small Piedmont watershed. In: H. Taylor et al., editors, Stable isotope geochemistry: A tribute to Samuel Epstein. Geochem. Soc., San Antonio, TX. p. 195–203.

West, A.G., S.J. Patrickson, and J.R. Ehleringer. 2006. Water extraction times for plant and soil materials used in stable isotope analysis. Rapid Commun. Mass Spectrom. 20:1317–1321. doi:10.1002/rcm.2456

Windhorst, D., P. Kraft, E. Timbe, H.-G. Frede, and L. Breuer. 2014. Stable water isotope tracing through hydrological models for disentangling runoff generation processes at the hillslope scale. Hydrol. Earth Syst. Sci. 18:4113–4127. doi:10.5194/hess-18-4113-2014

Wong, T.E., J. Nusbaumer, and D.C. Noone. 2017. Evaluation of modeled land–atmosphere exchanges with a comprehensive water isotope fractionation scheme in version 4 of the Community Land Model. J. Adv. Model. Earth Syst. 9:978–1001. doi:10.1002/2016MS000842

Zhao, P., X. Tang, P. Zhao, C. Wang, and J. Tang. 2013. Identifying the water source for subsurface flow with deuterium and oxygen-18 isotopes of soil water collected from tension lysimeters and cores. J. Hydrol. 503:1–10. doi:10.1016/j.jhydrol.2013.08.033